Groundwater recharge/discharge patterns and groundwater–surface water interactions in a sedimentary aquifer along the River Kitinen in Sodankylä, northern Finland

Susanne C. Åberg*, Kirsti Korkka-Niemi, Anne Rautio, Veli-Pekka Salonen and Annika K. Åberg

*University of Helsinki, Department of Geosciences and Geography, P.O. Box 64, FI-00014 Helsinki, Finland (*corresponding author's e-mail: susanne.aberg@helsinki.fi)*

Areas of groundwater–surface water interaction in riverbanks and open mires are important habitats for groundwater-dependent species. In order to preserve these ecosystems, the planning and development of mining operations on such locations require a fundamental understanding of the groundwater discharge–recharge and flow patterns. In this study, 3D flow modelling and a TIR survey were used to define the groundwater discharge. Simultaneously, the flow modelling and groundwater table fluctuation were used for defining groundwater recharge at a mining development site in northern Finland. The results indicated flow towards the River Kitinen and the discharge of groundwater in the banks of the river. The discharge also occurred within the mire area, which may provide suitable habitats for groundwater-dependent plant species. The modelling results and stable isotope variations indicated complex flow patterns and a potential groundwater connection from the Viiankiaapa mire through possible bedrock fractures to the river. Recharge mainly occurred in the sorted sediment accumulations of the riverbanks and partly also in the mire area.

Introduction

The boreal and subarctic regions of the Northern Hemisphere are sparsely populated and mostly in their natural state. The surficial deposits are mainly glaciogenic, and rivers and open mires dominate the hydrological systems (Lahermo 1970, Price and Maloney 1994, Laitinen *et al.* 2005). Rivers are an important component of runoff in northern Finland (Solantie and Ekholm 1985) and the river discharge is usually about 40–60% of the precipitation (Korhonen 2007).

Interactions between groundwater (GW) and surface water (SW) are an essential part of the hydrological cycle in river settings, as well as in mires. If the GW table is above the river stage, GW discharges into the river. According to Siegel (1988), a wetland is a GW discharge area if the GW movement is upwards from the underlying sediment and a recharge area when it is downwards. However, the fluxes in both directions can be occasionally limited due to the low hydraulic conductivity of peat. Mire hydrology and GW recharge/discharge patterns are crucial

for the mire vegetation, but the relationship has seldom been studied (Laitinen *et al*. 2005).

The complexity of the sedimentation of surficial deposits in central Lapland (Fig. 1) in northern Finland makes GW occurrences scattered and elusive. Glacial erosion has been weak within the ice-divide zone (Kujansuu 1967, Hall *et al*. 2015) and the till units from multiple glacial events as well as river and lake sediments (Hirvas 1991, Johansson and Kujansuu 2005, Salonen *et al*. 2014) have been preserved as relatively thick and complex sediment packages with varying hydraulic conductivity values and storage capacity (Salonen *et al*. 2014).

Northern Finland is the target area of intensive exploration activities due to its ore potential (Eilu 2012). The water management issues of the mining as well as mine development sites have been comprehensively discussed for years (Younger and Wolkersdorfer 2004, Kauppi *et al*. 2013, Salonen *et al*. 2014). To manage the environmental impacts of mining activities and to diminish the environmental risks, understanding of the hydrogeological conditions before the plan to mine is important. In particular, the study of waterbodies (SW bodies, aquifers and their connections) prior to the initiation of possible mining activities is considered a prerequisite for socially acceptable mining.

A Cu-Ni-PGE deposit named Sakatti was discovered in Sodankylä, northern Finland, in 2009 (Brownscombe *et al*. 2015), near the regulated River Kitinen and beneath the environmentally sensitive Viiankiaapa mire (Fig. 1). The mire is protected by the Natura 2000 network due to its extensive aapa-type mire environments with fen patches that are habitats for several endangered plant and bird species (Hjelt and Pääkkö 2006). Since the 1960s, the River Kitinen has been regulated by the hydroelectric power plants and reservoirs (Marttunen *et al*. 2004). The mining developments require a comprehensive understanding of the hydraulic environment of the Viiankiaapa mire and the River Kitinen, their connections to the aquifers nearby, as well as the effect of the river and its regulation on the Viiankiaapa mire.

Studies of the impact of GW–SW interaction, such as Winter (1999), Woessner (2000) and Sophocleous (2002) has increased drasti-

cally in the last decades (Fleckenstein *et al*. 2010), indicating their increasing influence. The GW–SW interaction of lakes and streams and the recharge/discharge patterns are also dependent on topography (Winter 1999). SW flow through the river bank (bank storage) affects the ratios of GW flux to the river. At the same time, the existence of an open mire close to the river complicates GW–SW interaction. These GW–SW interaction areas are important for GW-dependent ecosystems (GDE) (Triska *et al*. 1993, Sophocleous 2002) and the recognition of GDEs has become an objective required by law in Finland since 2014 (Act on Water Resources Management 1263/2014).

GW flow modelling can be utilized as a tool for understanding GW–SW interactions, as well as recharge/discharge patterns. According to the review of Barthel and Banzhaf (2016), the modelling of GW–SW interactions are commonly performed by GW flow models like the MODFLOW river package (Harbaugh 2005), with coupled SW–GW flow models like HydroGeoSphere (Therrien *et al*. 2010) or ParFlow (Kollet and Maxwell 2006), or loosely-coupled models like MIKE SHE (Hughes and Liu 2008). Barthel and Banzhaf (2016) noted that GW–SW processes at different scales need different aspects in the modelling and simplifying of the systems. In the larger scale, observing GW-SW fluxes in the riverbed need to be simplified, while on a detailed scale, the area beyond the riverbed needs to be simplified.

The temperature has been used as a GW−SW interaction tracer, since the GW temperature is relatively constant, while SW temperatures fluctuate diurnally and annually (Stoneman and Constantz 2003, Anderson 2005, Rautio *et al*. 2018). Low-altitude thermal infrared (TIR) imaging has been successfully utilized to identify and localize GW discharge into wetlands or water bodies (Torgersen *et al*. 2001, Dugdale *et al*. 2013, Rautio *et al*. 2018). In addition to TIR, the stable isotopes of oxygen and hydrogen ($\delta^{18}O$, δD) have been used for decades to verify the observed GW−SW connections when the end members sufficiently differ (Gat and Gonfiantini 1981, Krabbenhoft *et al*. 1990, Kendall and Coplen 2001, Rautio and Korkka-Niemi 2015). Recently, the stable isotopes of $\delta^{18}O$ and δD
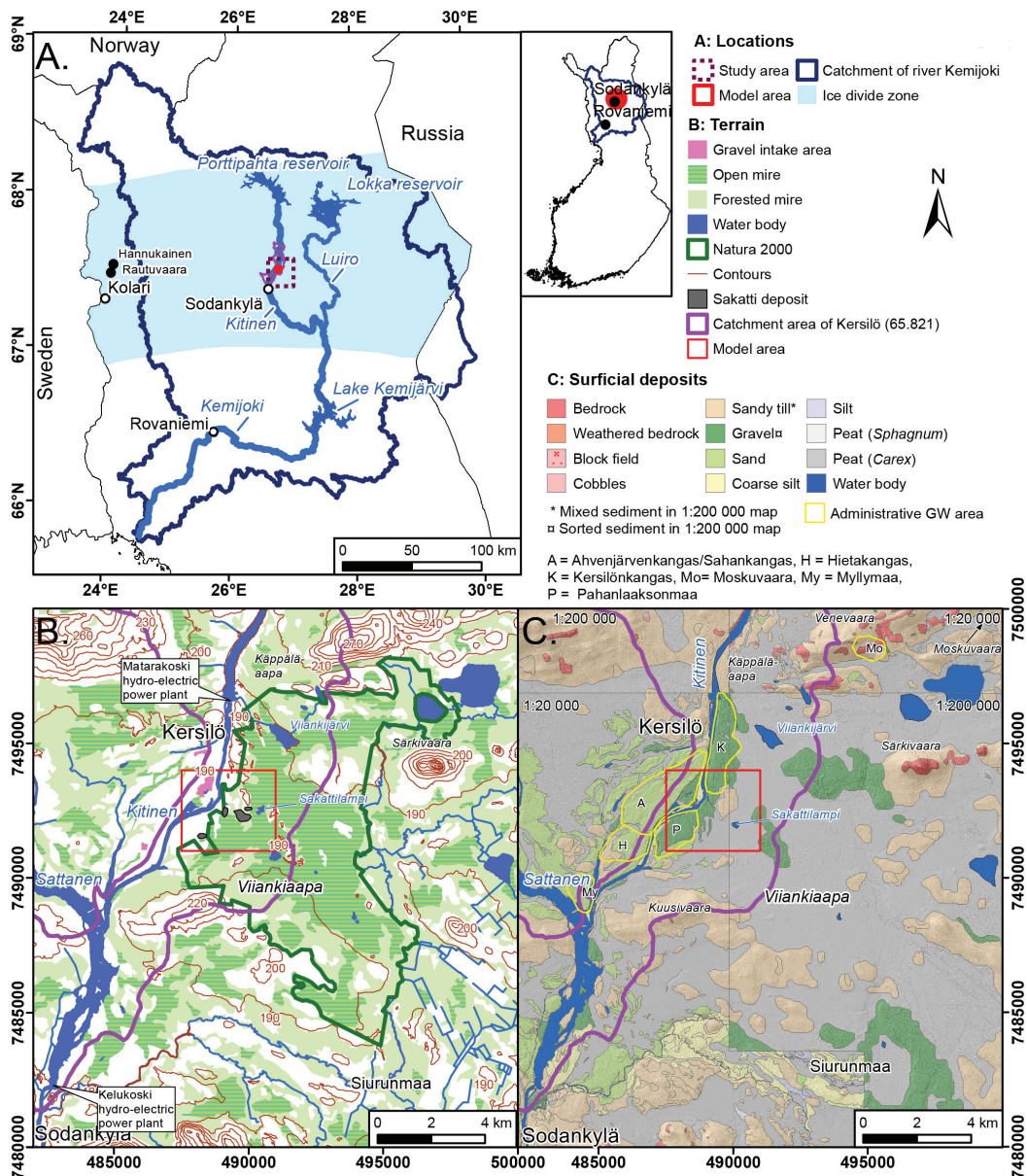
Fig. 1. **A**: The catchment of the Kemijoki River, including the River Kitinen and the Porttipahta and Lokka reservoirs, which are used to regulate the rivers. **B**: The study area and the border of the Natura 2000 conservation area. The two closest hydroelectric power plants are indicated in the figure. **C**: Surficial deposits and administrative GW areas of the study area. The Sakatti deposit is modified after Brownscombe et al. (2015). Base maps, terrain elements were reproduced with permission from the copyright owner (National Land Survey of Finland). Surficial deposits map were reproduced with permission from the copyright owner (Geological Survey of Finland). River, lake in Fig. 1a and catchment polygons and Administrative GW area were modified and reproduced with permission from the copyright owner (Finnish Environment Institute).

have been increasingly used to characterize the hydrology and GW–SW exchange of wetlands (Hunt *et al.* 1998, Clay *et al.* 2004, Marimuthu *et al.* 2005). In this study, TIR imaging, in situ temperature measurements and the stable isotopes of oxygen and hydrogen were used to validate GW flow modelling and to verify the GW discharge areas.

The aim of this study was to understand GW and SW interactions and their flow patterns in relation to GW-dependent ecosystems on the eastern flank of River Kitinen in Sodankylä, northern Finland, as a baseline study at a mining development site. It was hypothesized that the complex sedimentation environment affects the hydrology and hydrogeology of the mire and the recharge and discharge patterns, and simultaneously, the mire and its ecology are dependent on the discharging GW. 3D GW flow modelling, TIR imaging and the stable isotopic composition were utilized to define the GW flow patterns and the discharge and recharge areas.

Study area

Geological and hydrological background

The study area is located in the municipality of Sodankylä, in the western part of the Viiankiaapa mire (Fig. 1). The area is located close to the central Lapland ice-divide zone, which means that surficial deposits are thick and complex compared to the average in Finland (Johansson and Kujansuu 2005, Åberg A.K. *et al.* 2017a). The area is topographically relatively flat. The altitude of the mire is about 180–200 m above sea level (a.s.l.), with the highest hills in the area rising 50–90 metres above the surface of the mire.

The bedrock of the study area mainly consists of mafic and ultramafic volcanic rocks, quartzites, mica schists and gabbros (Tyrväinen 1980, Pulkkinen 1983, Tyrväinen 1983). The Proterozoic bedrock is partially fractured in the upper part (Hirvas 1991, Hall *et al.* 2015) and in some locations chemically weathered as well. It is overlain by Quaternary deposits mainly consisting of glacial, fluvial and aeolian clastic sediments and often covered with peat deposits

(Fig. 1c). The thickness of the unconsolidated sediment varies between 0–45 m with a median of 9.1 metres (Åberg A.K. *et al.* 2017a).

An approximately 1–6-metre-thick till overlies directly bedrock in the Kitinen valley and below the Viiankiaapa mire area (Åberg A.K. *et al.* 2017a). The till is covered with sorted sediments consisting of aeolian sands and fluvial deposits within the mire area and with fluvial sediments on the banks of the River Kitinen. The western bank of the river has alternating multiple tills and interlayering sandy deposits observed in the open sections of Kärväsniemi (Fig. 1b). The multiple till layers originate from separate Weichselian glacial events (Fig. 1a) (Åberg A.K. *et al.* 2017a). The aquifer-aquitard system can be complex due to existing subtill sands, gravels and gyttja layers, as described in Åberg A.K. *et al.* (2017a).

Rivers with their outwash plains are a central geomorphological feature in central Lapland. According to Lahermo (1973), outwash plains are the most abundant GW reservoirs of the area. Several minor aquifers also exist in the banks of the River Kitinen (http://www.syke.fi/avointieto [In Finnish]) (Fig. 1c). The most considerable of these aquifers is the Sahankangas aquifer (Fig. 1c), which is defined as an outwash plain (Räisänen 2014). The other minor aquifers are located in the eastern banks of the River Kitinen (Fig. 1c).

The most important hydrological systems of the area are the regulated River Kitinen and the protected Viiankiaapa mire. Viiankiaapa is a large, mainly treeless wetland with a well-developed flark and string pattern and fen patches (Pääkkö 2004, Hjelt and Pääkkö 2006). The hydrology of the aapa mire depends on the precipitation rate, GW and SW flow, spring flood and the rate of snowmelt (Ruuhijärvi and Lindholm 2006). The Viiankiaapa mire started to develop after the Late Weichselian deglaciation about 10 000 years ago (Lappalainen 1970, Suonperä 2016). According to Saarnisto (1992), the confluence of the River Kitinen and the Luiro River (Fig. 1) was formed at about the same time.

The River Kitinen is the largest tributary of Finland's longest river, the 552-km-long Kemijoki River (Marttunen *et al.* 2004) (Fig. 1).

Before the 1960s, the river was sensitive to flooding due to the small number of lakes within its large drainage system (Aalto 2008, Alanne *et al*. 2014). These floods enabled high biological diversity in the mire near the river banks (Karplund 1990). Water flow regulation via the Porttipahta and Lokka reservoirs (Fig. 1) since the 1960s has reduced the regular flooding of the River Kitinen (Alanne *et al*. 2014). A major change in the system within the study area was the construction of the Matarakoski hydroelectric power plant in 1995 (Fig. 1), which raised the river stage by seven metres above the natural stage (see Huokuna 1991). The average river discharge at the Matarakoski power plant is about 50–100 m^3 s^{-1} and the maximum rates vary from 200 to 400 m^3 s^{-1} (Kemijoki Oy 2017, unpubl. data). The annual runoff of the Kersilö watershed (Fig. 1) varied from 200 to 340 mm yr^{-1} during the years 2012–2015 and the maximum runoff was about 20 mm day^{-1} in the middle of May according to the watershed model (Vehviläinen 2007) of the Finnish Environment Institute (SYKE). The runoff rate was 40–55% of the precipitation.

Climate

The nearest weather station is in Sodankylä, 10 km south of the study area (Fig. 1). The mean annual temperature at Sodankylä is $–0.4$ °C and the June and January average temperatures are $+15$ °C and $–12$ °C, respectively (http://ilmatieteenlaitos.fi/vuositilastot [In Finnish]) (Appendix Fig. A1). The average annual precipitation in Sodankylä is 500–650 mm yr^{-1}, of which about half falls as snow, usually from November to May (http://ilmatieteenlaitos.fi/vuositilastot [In Finnish]). Mean evaporation was about 320 mm yr^{-1} between 1960 and 2011 (Moroizumi *et al*. 2014).

Endangered mire species within the area

The endangered ecosystems are mainly located in the fen patches of the Viiankiaapa mire. The habitats of four endangered or vulnerable GW-dependent species, *Hamatocaulis vernicosus* (vulnerable), *Hamatocaulis lapponicus* (endangered), *Meesia longiseta* (vulnerable) and *Saxifraga hirculus* (endangered) (Kulmala 2005, Eurola and Huttunen 2006), have habitats close to the Sakattilampi pond (http://www.syke.fi/avointieto [In Finnish]) in the Viiankiaapa mire (Fig. 1B). Sakattilampi is located inside the exploration permit area of the mining company AA Sakatti Mining Oy (Fig. 1b). The habitats of these four plant species usually indicate GW discharge (Kulmala 2005, Eurola and Huttunen 2006).

Materials and methods

General

The study was conducted in six steps and explained in more detail below (Fig. 2). First, the hydrostratigraphic units of the model area (Fig. 1) were defined. Second, the hydraulic conductivities were defined for the units of a 3D hydrostratigraphic model and the model was converted into a numerical 3D GW flow model. Third, the initial head was estimated from GW table observations, ground penetrating radar (GPR) profile interpretations (Appendix Fig. A2) and the SW altitudes, which were defined from LiDAR DEM (Light Detection and Ranging Digital Elevation Model) and orthoimage interpretations. Fourth, GW recharge and annual GW table fluctuations were studied from GW table data obtained from monitoring wells. Fifth, the flow model was calibrated with the GW and SW observations, and GW discharge zones were defined from TIR data and stable isotope studies. Sixth, the model results were compared with GW discharge observed from TIR images and with the occurrences of endangered species.

Definition of preliminary 3D hydrostratigraphy

A simplified and modified version of Quaternary sediments and bedrock topography (hereafter: 3D geological model), described in detail in Åberg A.K. *et al*. (2017a), was utilized as the basis for the definition of a 3D hydrostrati-
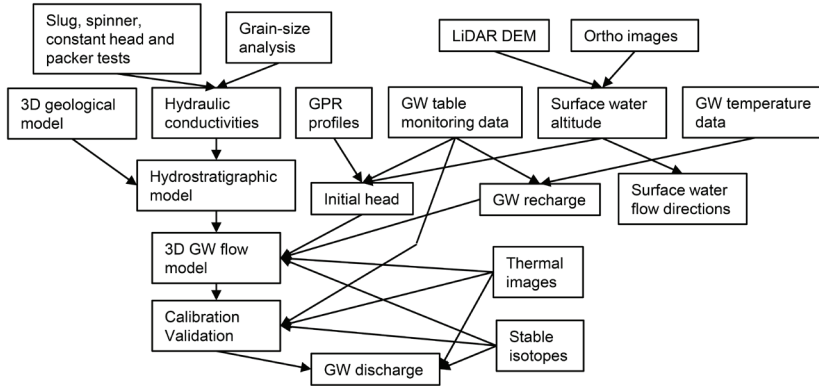
Fig. 2. The relationships between the materials and methods used in this study.
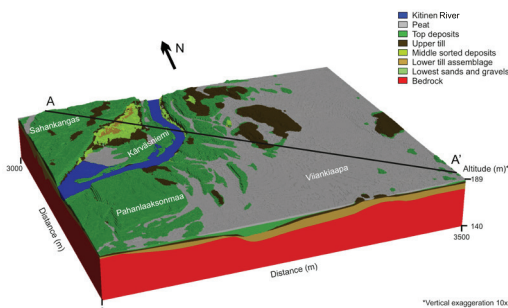

Fig. 3. An eight-layered, 10 × 10 m cell-sized MOD-FLOW grid created from the simplified and modified 3D hydrostratigraphic model based on Åberg A.K. *et al.* (2017a). Hydrostratigraphic units were used as parameter zones in the 3D GW flow model. River Kitinen and Peat on the top layer were used for the "open water and mire" recharge zone and other units of the top layer for the "forested area" recharge zone.

graphic model (Fig. 3). The primary 3D modelling software used was Leapfrog Geo ver. 4.0 (Seequent Ltd.). The horizontal resolution of the model was 10 × 10 metres. The flow modelling was used to evaluate and improve the existing geological model (Åberg S.C. *et al.* 2017b).

Calculation of hydraulic conductivities

The hydraulic conductivities of the hydrostratigraphic units were estimated by using grain-size analysis of soil samples and slug tests (Appendix Fig. A2, Table 1). AA Sakatti Mining Oy installed 24 GW monitoring wells in the Viianki-aapa mire area (Golder Associates 2012, unpubl. data) in 2012; and 17 of the wells have automatic

stations for continuous monitoring of water level and water temperature ever since. Twelve of them were well triplets that had three adjacent wells installed in different depths (Appendix Fig. A2). During the drilling of the monitoring wells, sediment samples were taken and the grain-size distribution of 14 samples was analysed in the soil laboratory of Geobotnia Oy (Golder Associates 2012, unpubl. data). Slug tests were also performed from 12 monitoring wells in 2012 (Golder Associates 2012, unpubl. data). In addition, four new test sites were excavated near Moskuvaarantie, and in the gravel intake area of Kärväsniemi in 2015, and at the same time, 14 new sediment samples were taken for grain-size analysis to calculate the hydraulic conductivities (*k*-values). *k*-values were calculated by applying the Sauerbrei method (Sauerbrey 1932, Vukovic and Soro 1992):

$$k = \beta \frac{gn^3}{v(1-n)^2}(d_{17})^2, \qquad (1)$$

where β is 3.75×10^{-3}, g is 9.81 m s^{-1}, v is the kinematic viscosity of water, n is porosity and d_{17} is the effective grain size. *k*-values are expressed in m s^{-1} at T (temperature) = 5 °C. Even though the method is most suitable for sands and silty sands, Hänninen *et al.* (2000), for example, have previously used it to calculate the *k*-values of tills.

In addition, hydraulic conductivities of the fractured zone of the bedrock were estimated based on the results of hydrogeological testing from boreholes including constant head, spinner

Table 1. Calculated hydraulic conductivities and the interpreted deposit type of the sediment samples. Depth indicates the coring depth of the sediment sample, Sed. type (lab) indicates the laboratory definition of the sediment type, Sed. type (interpreted) indicates the final interpretation of the sediment type, Screen unit indicates sediment type of the screen of the monitoring well, d^{17} indicates the grain size d^{17} in the grain-size analysis, k (m s⁻¹) Sauerbrei indicates hydraulic conductivity calculated with the Sauerbrei method and k (m s⁻¹) and Slug is the hydraulic conductivity estimated with the slug test.

Sample	Depth (m)¤	Sed. type (lab)	Sed. type (interpreted)	Screen unit (depth m)	d^{17} (mm)	k (m s⁻¹) Sauerbrei#	k (m s⁻¹) Slug*
GA102			Peat	Peat (1-3)			3.0×10^{-6}
GA103			Peat	Peat (1–2)			5.4×10^{-5}
GA104			Peat	Peat (2–4)			3.7×10^{-6}
GA200Hk	3.8-5.8	Sandy till	Sand	Sand (4.5–6.5)	0.074	7.3×10^{-6}	3.6×10^{-5}
GA201Hk	3-5	Sandy till	Sandy till	Till (3–5)	0.020	5.3×10^{-7}	
GA202Hk	2.5-4.5	Gravelly sand	Sand	Till (4–5)	0.214	2.0×10^{-4}	1.6×10^{-6}
GA202Mr	4.5-5.8	Gravelly sandy till	Gravelly sandy till	Till (4–5)	0.032	1.4×10^{-6}	
GA203	3-5	Sandy gravel	Sandy gravel	Gravel (3.5–6)	0.375	6.0×10^{-4}	
GA204	3.5-5.5	Sandy gravel	Gravelly sandy till	Gravelly till (2–4)	0.175	1.3×10^{-4}	3.4×10^{-7}
GA205Hk	2-4	Sandy gravelly till	Sandy gravelly till	Sand (2–4)	0.091	1.1×10^{-5}	
GA300			Sand	Sand/gravel (3–4)			1.7×10^{-6}
GA301	7.5-9.5	Sandy gravelly till	Sand	Sand/gravel (7.5–9.5)	0.188	1.5×10^{-4}	
GA302	7.5-9.5	Gravelly sandy till	Gravelly sandy till	Sand/gravel (8–10)	0.030	1.2×10^{-6}	
GA303	10-12	Silty sandy till	Silty sandy till	Till (10.5–12.5)	0.013	2.2×10^{-7}	8.3×10^{-6}
GA304HkMr	12-14	Sandy till	Sandy till	Till (12–14)	0.019	4.9×10^{-7}	6.6×10^{-7}
GA304SiMr	14-16	Sandy till	Sandy till	Till (12–14)	0.030	1.2×10^{-6}	
GA305	8-10	Gravelly sandy till	Gravelly sandy till	Till (8–10)	0.020	5.3×10^{-7}	
GA306	4-6		Till	Sandy till (3–5)			3.1×10^{-6}
GA400			Bedrock	Sheared bedrock (5–7)			1.6×10^{-5}
GA402Hk	4.5-5.5	Gravelly sand	Gravelly sand	Bedrock (11–13)	0.224	2.2×10^{-4}	
GA404			Bedrock	Bedrock (8.5–10.5)			5.3×10^{-6}

Table 1. (*continued*)

Sample	Depth (m)¤	Sed. type (lab)	Sed. type (interpreted)	Screen unit (depth m)	d_{17} (mm)	k (m s^{-1}) Sauerbrei[#]	k (m s^{-1}) Slug[*]
TS1/2015 UNIT2A	3.7-5.3	Sandy gravel	Sandy gravel		0.5	1.1×10^{-3}	
TS1/2015 UNIT2B	3.7-5.3	Sandy gravel	Sandy gravel		1	4.3×10^{-3}	
TS1/2015 UNIT3	2.7-3.7	Gravelly till	Gravelly till		0.25	8.3×10^{-5}	
TS1/2015 UNIT4	1.2-2.7	Sand	Sand		0.5	1.1×10^{-3}	
TTS1/2015 UNIT5	0.2-1.2	Sandy till	Sandy till		0.045	2.7×10^{-6}	
TS2/2015 UNIT1	5.3-6.3	Sandy till	Sandy till		0.08	8.5×10^{-6}	
TS2/2015 UNIT3	4.3-5.2	Sandy gravel	Sandy gravel		1	4.3×10^{-3}	
TS2/2015 UNIT4	3.9-4.3	Gravel	Gravel		2	1.7×10^{-2}	
TS2/2015 UNIT5	2.3-3.9	Sand	Sand		0.25	2.7×10^{-4}	
TS2/2015 UNIT6	1.9-2.3	Sandy till	Sandy till		0.125	2.1×10^{-5}	
TS2/2015 UNIT7	0.7-1.9	Gravel	Gravel		1	4.3×10^{-3}	
TS2/2015 UNIT8	0.3-0.7	Sand	Sandy till		0.045	8.7×10^{-6}	
TS–3/2015	0-2.2	Sandy till	Sandy till		0.02	5.3×10^{-7}	
TS–4/2015	0-1.5	Sandy till	Sandy till		0.016	3.4×10^{-7}	

¤ Represents unit depth, not actual sample depth, which is unknown

Calculation method from Sauerbrey (1932)

*k-value calculated by geometric mean of slug test solutions of Hvorslev (1951) and Bouwer and Rice (1976)

and packer tests (SRK 2019, unpubl. data) and two slug tests (Golder Associates 2012, unpubl. data). The boreholes were open bedrock holes including steel casing from the surface to fairly competent rock. The lower part of casing was cemented to isolate the surficial deposits and topmost weathered bedrock from fairly competent/complete bedrock.

Modelling the 3D GW flow

Definition of the initial head

The preliminary estimations of GW table altitudes were performed with ArcMap (ESRI) and Leapfrog. First, the interpolation of the GW tables on the selected days of 1 Apr., 1 May, 15 May and 1 June 2014, due to these having the most complete monitoring data. The data was tested using the natural neighbour method (Sibson 1981) with ArcMap to examine the maximum variation in the spring season. In addition, a more complete 3D GW table representing 15 Aug. 2015 was generated with Leapfrog for use in 3D GW flow modelling. The data used for the 3D GW table were the altitudes of flarks and springs, GW table observations, interpretations of the GW table from GPR profiles from the field campaigns in April and August 2015 and the interpolated contours of the GW table (Appendix Fig. A2). The field studies of 2015 also included manual measurements from monitoring wells in gravel intake areas ($n = 4$), the GW1 monitoring well near Matarakoski and minipiezometer measurements ($n = 3$) on the eastern shore of the River Kitinen (Appendix Fig. A2). The GPR-interpreted GW tables had about 0.5 m error due to uncertainties in time to depth conversions (Åberg A.K. *et al.* 2017a) and about 2.1–0.7 m error depending on the depth of the GW table caused by the antenna separation with the distance of 4.2 m. However, due to the shortage of data points, the modelling of the 3D GW table was enforced with 100/200 m interval sections of hand-drawn polylines.

Description of the 3D GW flow model

The 3D hydrostratigraphic model generated with Leapfrog was converted into a MOD-FLOW-2005 grid (Fig. 3). The model editing was performed with ModelMuse graphical user interface (GUI) software (UGSG). The modelling code was changed to MODFLOW-NWT (Niswonger *et al.* 2011) due to its capability of modelling unconfined aquifers with highly varying layer thicknesses. The code uses a Newton formulation and the Upstream-Weighting (UPW) Package for unconfined aquifer solutions (see Niswonger *et al.* 2011). The 3D GW flow model was a steady-state model with eight layers. The water budget was calculated for one year. The upper-six layers and the river were modelled as convertible aquifers (changing from the unconfined to the confined condition was possible within a layer), and the bedrock layer was modelled as a confined aquifer. Horizontal hydraulic conductivity (HK) parameters were defined for the eight hydrostratigraphic units (Fig. 3). Vertical hydraulic conductivity was defined as the ratio of horizontal to vertical hydraulic conductivity with vertical anisotropy (VANI) parameters. Anisotropy was assumed to be 10 due to horizontally stratified sediments except 100 in peat acrotelm and catotelm (Reeve *et al.* 2000) and 1 in the bedrock to keep converging of the model possible. The horizontal grid resolution of the model was 10 × 10 m. The minimum thickness of a grid cell was 0.2 m. The grid was modified from a Leapfrog-generated grid as follows: the river top was reduced to 0.2 metres above the bottom of the river. The head of the river was interpolated with trend interpolation in ArcMap due to rugged river surface in LiDAR DEM. Simultaneously, layer 1 at the bottom of the mire area was modified to present two-thirds of overall peat thickness as the acrotelm of the mire based on the observed thickness in peat drillings. The original layer 2 bottom was then presenting the bottom of catotelm. The bedrock bottom was modified to represent the bottom of the upper fractured/weathered zone to the average depth of 35 m from the bedrock surface based on bedrock drillings. The fractures of the bedrock were added as separate parameter zones within the bedrock with polylines derived from the map of the report of the environmental impact assessment of the Sakatti project (http://www.ymparisto.fi/sakatinkaivosYVA [In Finnish]). As the overall schistosity of the bedrock and the

major faults and fractures are almost vertical, the simplification of the fractures and faults and vertical zones within one layer was possible. It was assumed that the fracturing/weathering rate affects more to the hydraulic conductivity than the bedrock type.

Boundary conditions were defined as follows: The River Kitinen was modelled with the RIV package, and the conductance was calibrated. Recharge was simulated with the RCH package with two different zones: the "open water and mire" zone (RCH_Par2) and "forested areas" zone (RCH_par1) (Fig. 3). The recharge rate in the open water and mire zone was assumed spatially uniform. The water table fluctuation (WTF) method (Meinzer 1923) was used to roughly estimate the recharge rate related to spring thaw in the proximity of the monitoring wells for the forested area zone (Appendix Fig. A2). The recharge from precipitation was estimated with the episodic master recession curve method (EMR) (Nimmo *et al*. 2015). Specific yields were estimated based on the definitions of Johnson (1967). The sum of recharge from WTF and EMR method were converted to precipitation-to-recharge ratios (see Nimmo *et al*. 2015), which were then used as multipliers for the RCH parameter. The parameter value was set to the precipitation rate of the hydrological period from October 2013–October 2014. It was assumed that recharge is a certain proportion of the precipitation and the spring thaw, which depends on the properties of the location. The varying multipliers were used to gain spatial heterogeneity to recharge due to variable hydraulic conductivities of surficial deposits and the multipliers were interpolated within the forested area zone. The drain (DRN) package was used to cover the mire area and the gravel intake area to simulate possible discharge. The DRN conductance was calibrated and the constant head boundaries were added to borders that have a constant input of water due to the extensive open mire areas surrounding the model area. Their starting heads were extracted from the Leapfrog-generated 3D GW table, assuming that it is close to the long-term average head. Head-dependent flux boundaries were added in Sahankangas and Pahanlaaksonmaa as outer limits of the model. The heads were estimated based on the levels of

Koistamonpulju mire (Appendix Fig. A2) and the River Kitinen, respectively. Their conductance was calculated with the estimated *k*-value multiplied by the cross-sectional area of grid cells divided by the distance to the real boundary condition location. However, the model itself was set to present the hydrological year from October 2013 to October 2014 due to the higher-than-average precipitation and estimated recharge rate of the following year (2015), which included the recharge from snow accumulation of 2013.

Calibration and validation of the 3D GW flow model

During the model development, different hydraulic conductivity zonings for the HK parameters were tested to find the best solution to match the simulated GW table with the head observations. Simultaneously, the structures of the 3D geological model and the 3D hydrostratigraphic model were reconstructed twice during model calibration by changing the thicknesses and the distributions of the layers. The hydraulic conductivities of the unit's top deposit, upper till, middle sorted deposits, lower till and bedrock (Fig. 3) were interpolated with the natural neighbour method from the results of the grain-size analyses, spinner, constant head, packer and the slug tests to the corresponding HK parameter zones by using multipliers. The units with less than three *k*-value measurements (Kitinen, peat, and lowest sands and gravels) had constant *k*-values. In addition, dummy points were added during model development to enforce more accurate results for the interpolated *k*-values. The fracture and fault *k*-values, RIV and DRN conductance were estimated with automatic parameter estimation with PEST (Doherty 2015). The starting value to fractures, faults, RIV conductance and DRN conductance were 1×10^{-3}, 1×10^{-6}, 1×10^{-5} and 3.7×10^{-8}, respectively. The minimum limit was 1×10^{-10} to keep the model convergence possible and maximum limit was 1×10^{-2} for all calibrated parameters. The initial DRN conductance was estimated from average of peat *k*-values divided by 100 (VANI) and river conductance was an estimation of the average
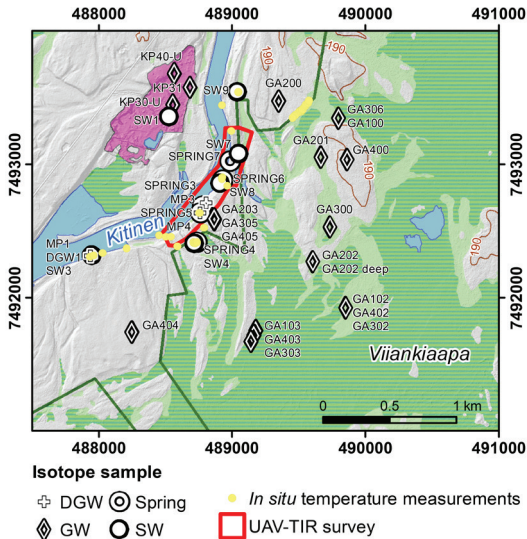
Fig. 4. The coverage of the UAV-TIR survey conducted on 29–30 Jul. 2017, the field temperature measurements and the stable isotope sampling locations in Aug. 2015 and Sep. 2016. DGW = discharging GW. Terrain elements were reproduced with permission from the copyright owner (National Land Survey of Finland)

k-value of river bottom that was assumed to be a mixture of sand, gravel and till. Selected average GW table observations from monitoring wells in 2014 ($n = 15$), springs ($n = 4$) and open-water bodies including SW points and flarks ($n = 84$) calculated from the LiDAR DEM and one discharging GW point were used as GW table calibration points with the head observation (HOB) package. The GPR observations were excluded during calibration due to their high uncertainty in velocity corrections.

Description of the hydrological data

Hydrological data, including precipitation, the snow water equivalent (SWE), river stage and river discharge were collected to investigate the water budget and recharge rates. Precipitation data from 2012 to spring 2016 and SWE data from three winters in 2013–2014, 2014–2015 and 2015–2016, both data types from the geophysical observatory of Sodankylä, were used to estimate the recharge rates. River discharge and stage data were collected from the hydroelectric power plants at Matarakoski and Kelukoski (constructed

in 2001) (Fig. 1b) in order to examine the annual variation of the river stage and whether it affects the GW table. According to Golder Associates (2012, unpubl. data), river discharge shows no clear response to precipitation due to the dominating effect of snowmelt runoff and the regulation of the flow regime in the River Kitinen.

GW table fluctuations in monitoring wells

GW table data (measured every half an hour) from the monitoring wells were statistically examined with cross-correlation in order to understand the GW recharge patterns. The calculations were executed with Microsoft Excel 2016, SPSS ver. 24 (IBM Analytics) and Matlab ver. R2017b (MathWorks) scripts. The daily and annual averages of the GW table were calculated from the monitoring data. Cross-correlations of the daily average of the GW table with precipitation and SWE data were tested. In addition, new GW table observations from several monitoring wells were measured in the Kärväsniemi gravel intake area in August 2015 to estimate the GW table altitude and depth in the western banks of the River Kitinen (Appendix Fig. A2). Simultaneously, the cross-correlation between selected monitoring wells was also tested.

TIR survey and field temperature measurements

In northern Finland, the temperature of SW is higher than that of the discharging GW in the summer, and the GW flux into SW bodies and the land surface can, therefore, be observed as cold anomalies from TIR images. GW discharge sites were identified using an unmanned aerial vehicle (UAV) with TIR and RGB cameras (hereafter UAV-TIR) to examine selected locations in shoreline areas of the River Kitinen in July 2017 (Fig. 4). A FLIR TAU2 640 TIR camera integrated with a ThermalCapture module (TeAx Technology UG) was mounted on a Matrice 100 (DJI) together with a X3 RGB camera (DJI). The FLIR TAU2 640 had a pixel resolution of 640 × 512, a spectral range of 7.5–13.5 μm and a field of view of 45° × 37°. The system was capable of detect-

ing temperature differences of ±0.05 °C with an accuracy of ±5.0 °C or ±5.0% SE of the reading, as reported by the manufacturer.

A UAV-TIR survey was acquired from 100 m above the ground surface (a.g.s.), and the ground speed was approximately 3.5 m s^{-1} following the pre-set flight route points in the MapsMadeEasy mobile map pilot application (Drones Made Easy). Thermal images were collected digitally and recorded from the sensor to the ThermalCapture module at a rate of 8 frames per second, which guaranteed over 90% overlap along the track and 70% side overlap. The thermal image frames were tagged with coordinate data by a ThermalCapture GPS Receiver based on the u-blox 8 Multi GNSS UBX-M8030-KT chipset. The thermal image files were post-survey processed, mosaicked and interpreted with ThermoViewer ver. 2.1.5 (TeAx Technology UG), Pix4Ddesktop (Pix4D) and ArcMap ver. 10.3.1 (ESRI) software, respectively.

The flight altitude of 100 m a.g.s. produced a ground resolution of 13 cm. The UAV-TIR survey was carried out from 29–30 July 2017 and weather conditions varied between clear sky and partial cloud cover and air temperature from 20.2–24.9 °C (Sodankylä weather station, FMI). Altogether, the UAV-TIR survey covered 24 hectares of the riparian areas alongside the River Kitinen (Fig. 4).

The kinetic water temperature was measured 2 cm below the water surface with a sediment temperature probe (Therma Plus, Electronic Temperature Instruments Ltd, Worthing, West Sussex, UK, resolution: 0.1/1 °C accuracy: ±0.4 °C ±0.1% SE). Temperature measurements (n = 36) were collected simultaneously with water sampling in 2015 to examine the temperature variability and compare the water temperature values with the stable isotope composition of the water samples.

Stable isotopes

Water sampling under low-flow conditions was performed at selected field study sites (Fig. 4) in August 2015 and September 2016 to explore the connection between anomalous water temperatures and the stable isotope composition, to assess the level of GW−SW interaction and to verify/validate the modelled GW discharge indicated by the GW flow model. Observation well isotope samples (n = 6) from 2016 were included in the isotope dataset to gain more information on the spatial variability in the isotope composition of GW in the research area. The SW (n = 6) and spring water (n = 5) samples were collected directly from the river/brook channels and springs. GW samples (n = 21) from observation wells were taken with a bailer. Mini-piezometers were hand driven into the channel bed at the study sites using the method described by Lee and Cherry (1979) to sample the discharging GW (DGW; n = 4). The middle points of the mini-piezometer screens were at depths ranging between 24 and 164 cm below the surface of the channel bed.

The samples for stable isotope analysis were collected into 50-ml, high-density polyethylene bottles and preserved in a refrigerator until analysis. The stable isotope compositions (δ^{18}O and δD) were analysed from 36 samples collected during the field campaign in 2015 and 2016 (Fig. 4). Samples were filtered (0.2 μm and 0.8 μm in 2015 and 0.45 μm in 2016) and analysed with a Picarro L2120-I analyser at the Department of Geosciences and Geography, University of Helsinki. The isotope results are reported as δ values, representing a per mill (‰) difference relative to the international Vienna Standard Mean Ocean Water (VSMOW) standard. The δ^{18}O or δD values are defined as [(Rsample = Rstandard/−1](1000), where R refers to the ^{18}O/^{16}O or D/H ratios in both the sample and standard. The precision for a single analysis was ≤ 0.5‰ for δD and ≤ 0.1‰ for δ^{18}O. A deuterium excess (*d*-excess) of 10‰ is the average value for global precipitation and characterizes the meteoric conditions prevailing in the initial moisture source (Merlivat and Jouzel 1979). An index of the evaporation effect for each sample was calculated using the *d*-excess, determined as followed (Dansgaard 1964):

$$d\text{-excess} = \delta\text{D} - 8\delta^{18}\text{O}. \qquad (2)$$

SW flow directions

SW flow directions were defined with ArcMap by using orthoimages of NLS and a two-metre-
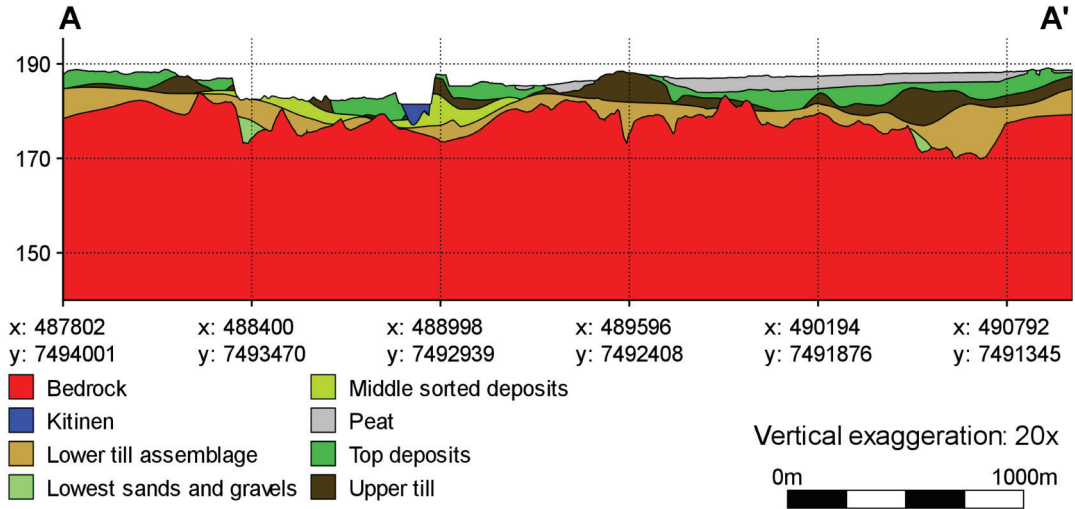
Fig. 5. Cross-section A–A' (Fig. 3, location) of the 3D hydrostratigraphic model.

resolution LiDAR DEM of NLS to study SW divides for understanding to relations to GW dependent mire species and evaluation of the GW flow model. The locations of SW bodies, including rivers, brooks, flarks and lakes, were picked from orthoimages as point data and their altitudes were calculated from the LiDAR DEM. The point data were used to create a surface of triangular irregular networks (TIN) that demonstrates the SW altitude. The TIN surface was converted into a raster and, the raster was used to create one-metre contours of SW bodies to study the flow directions. Flow directions were defined from the observed flow directions of the rivers and the brooks from base maps of NLS and using the assumption of Foster *et al.* (1983) that water flow in a mire is perpendicular to flarks and strings. The flow directions of areas lacking brooks and flarks were estimated using the created SW altitude contours, assuming that water flows towards the minimum altitude.

Results

Hydraulic conductivity of surficial deposits

The hydraulic conductivities vary from 2.2×10^{-7}–1.7×10^{-2} m s^{-1} (Fig. 1) in the study area,

being higher in gravels (1.1×10^{-3}–1.7×10^{-2} m s^{-1}) and sands (1.7×10^{-6}–1.1×10^{-3} m s^{-1}) and lower in tills (2.2×10^{-7}–8.3×10^{-5} m s^{-1}) (Fig. 5). However, some of the sandy and gravelly till units have relatively high hydraulic conductivities of 2.1×10^{-5}–8.3×10^{-5} m s^{-1}. Hydraulic conductivities are slightly higher in the gravel intake area in Kärväsniemi (Appendix Fig. A2) on the western side of the river (tills: 2.7×10^{-6}–8.3×10^{-5}, sands: 2.7×10^{-4}–1.1×10^{-3} and gravels: 1.1×10^{-3}–1.7×10^{-2}) than on the eastern side (tills: 2.2×10^{-7}–1.1×10^{-5}, sands: 1.7×10^{-6}–2.2×10^{-4} and gravels: 6.1×10^{-4}).

GW table and flow modelling

The GW flow direction is towards the River Kitinen and the GW table varies between 180.4–187.9 m a.s.l. (Appendix Fig. A2). The GW table is lower and its range is higher in monitoring wells near the river than in other wells (Fig. 6). The calculated *k*-values and the model definition indicate that the variety of *k*-values within hydrostratigraphic units (Fig. 3) is considerable (Fig. 2, Appendix Fig. A3). The *k*-values of tills are markedly lower beneath the mire area on the eastern side of the river than on the banks of the River Kitinen (Appendix Fig. A3). The flow model confirms that the major
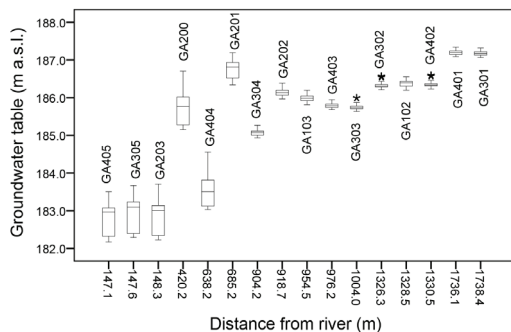
Fig. 6. Annual GW table ranges in 16 monitoring wells in 2014 presented as box-plot diagrams compared with the perpendicular distance from River Kitinen.

Fig. 7. Contour map of the calibrated GW table compared to the observed GW table. LiDAR DEM was modified and reproduced with permission from the copyright owner (National Land Survey of Finland). Water bodies were reproduced with permission from the copyright owner (National Land Survey of Finland).

flow direction is towards the River Kitinen, with a minor north-to-south component (Fig. 7), as also seen in the GW head observations (Appendix Fig. A2).

GW recharge

The GW recharge periods occurred during the years from 2012–2015, from the end of April until the end of September. The recharge in spring was related to the spring thaw and the recharge in summer and autumn was related to the higher precipitation rate (Fig. 8). The estimated recharge rate varied from 3.3×10^{-9} m s^{-1} to 1.2×10^{-8} m s^{-1} in the hydrological year from October 2013 to October 2014 (Fig. 2). The recharge rate was 10–69% of the precipitation (560 mm month^{-1}) of the hydrological year from October 2013 to October 2014 in forested areas and 19% of this in open water and mire areas. The maximum observed change in the GW table was over 1.4 m in well GA200.

TIR survey and field temperature measurements

The observed thermal anomalies in the study's 24 hectares area were classified into three categories and similar to previous studies (Rautio 2015, Rautio *et al.* 2015, Rautio *et al.* 2018): discrete or multiple springs, cold creeks/tributaries discharging into the River Kitinen and diffuse seepage anomalies. The final number of
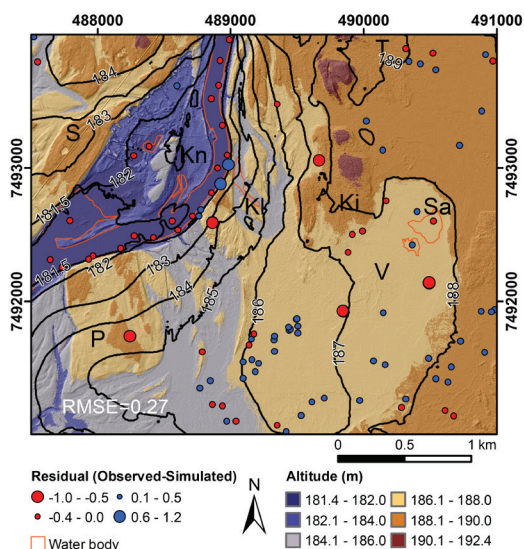
identified anomalies was 15, comprising of nine springs, one creek (Ruosteoja creek) and five diffuse seepage areas (Fig. 9). Contiguous GW seepage was detected along the eastern River Kitinen shoreline at the Kärväskoski location and was composed of several individual springs and diffuse seepage areas based on the UAV-TIR data (Fig. 9). This was also supported by the findings during the field campaign, such as large springs and more contiguous GW seepage areas on the eastern shoreline of the River Kitinen.

Stable isotopes

The measured mean δ^{18}O, δD and *d*-excess values of the water samples are presented in Appendix Table A4. There were significant differences in the stable isotope composition between the studied GW observation wells and springs (Fig. 9b and Appendix Table A4). The measured mean δ^{18}O, δD and *d*-excess values for all GW observation well water samples ($n = 21$) were –13.11‰, –99.2‰ and 5.7‰, respectively. The GW observation wells in the study area can
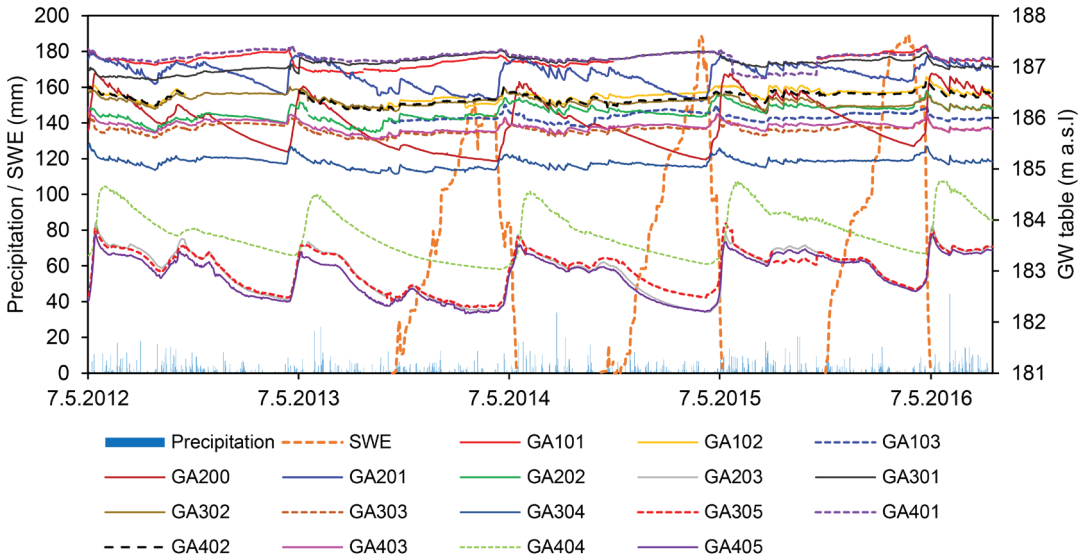
Fig. 8. Comparison of snow water equivalent (SWE) and precipitation with GW table fluctuations from 2012–2016. Hiatuses in the GW table data indicate removed data that were erroneous due to water sampling. Short-term GW fluctuations appear to follow rainfall events, especially in the wells located in the mire area.

Table 2. The parameters used in the calibrated GW flow model. HK presents horizontal *k*-values of a hydrostratigraphic unit. All parameters, excluding VANI (dimensionless ratio) and conductance ($m^2\ s^{-1}$), are presented as $m\ s^{-1}$.

Parameter name	Group	Description	Parameter value	Multiplier minimum	Multiplier maximum	VANI[□]
Kx2	HK	Kitinen	1.0×10^{-2}			1
Kx6	HK	Peat acrotelm	5.4×10^{-5}			100
Kx62	HK	Peat catotelm	1.0×10^{-6}			100
Kx7	HK	Top deposit	1*	1.2×10^{-6}	6.1×10^{-4}	10
Kx8	HK	Upper till	1*	5.3×10^{-7}	1.3×10^{-4}	10
Kx5	HK	Middle sorted deposits	1*	1.3×10^{-4}	4.3×10^{-3}	10
Kx3	HK	Lower till assemblage	1*	2.2×10^{-7}	8.3×10^{-5}	10
Kx4	HK	Lowest sands and gravels	1.5×10^{-4}			10
Kx1	HK	Bedrock	1*	2.7×10^{-8}	6.5×10^{-5}	1
Frac	HK	Bedrock fractures	1.4×10^{-3}			1
Faul	HK	Bedrock faults	4.2×10^{-5}			1
DRN_Par1	DRN	Drain conductance	2.3×10^{-5}	100$		
RCH_Par1	RCH	Recharge	$1.8 \times 10^{-8\#}$	0.13	0.69	
RCH_Par2	RCH	Recharge	3.3×10^{-9}			
RIV_Par1	RIV	River conductance	7.6×10^{-6}	100$		

*Hydraulic conductivity is calculated by interpolation with the natural neighbour method from multipliers
[□]Ratio of horizontal to vertical hydraulic conductivity
#Calculated from precipitation sum of October 2013–October 2014.
$Condfact factor that bases on 10 × 10 grid cell size. Conductance value is the product of the parameter value and the Condfact factor (see Harbaugh (2005))
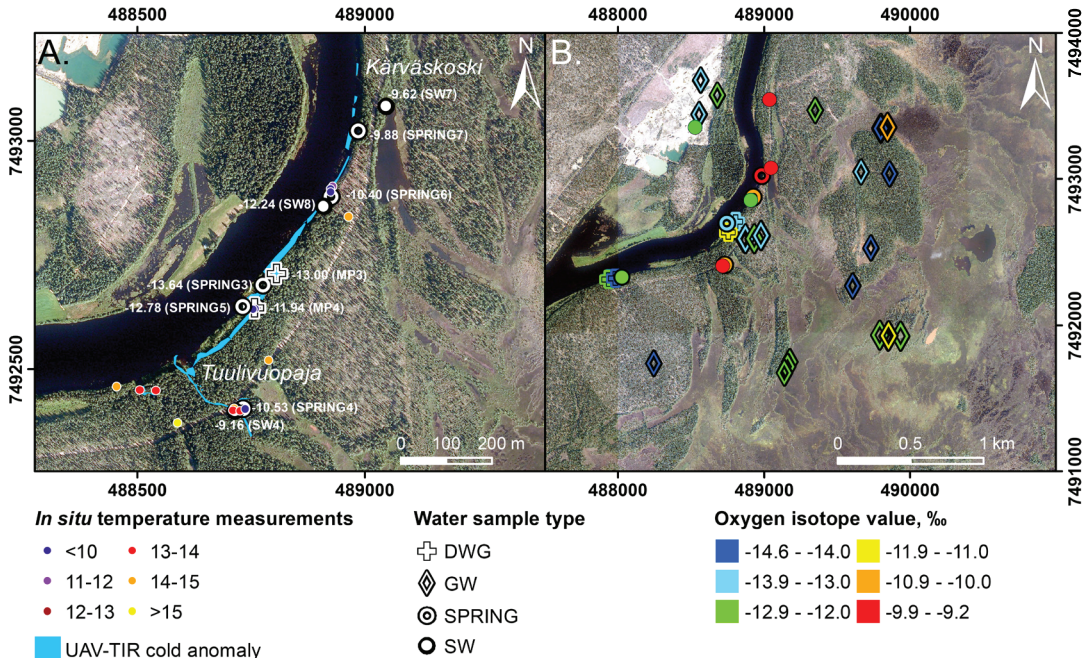
Fig. 9. **A**: Cold anomalies observed from thermal mosaic images, stable isotope values of oxygen in samples and in situ temperature measurements. **B**: Oxygen isotope values of water samples of the model area. Orthoimages were reproduced with permission from the copyright owner (National Land Survey of Finland).

be divided into three landform groups: (1) GW observation wells (n = 9) in forested areas/bog crests or in close proximity to these features; (2) GW observation wells in open mire/flark areas (n = 6); and (3) GW observation wells in the proximity of the River Kitinen (n = 6). The measured mean δ^{18}O, δD and d-excess values for these three groups were –13.63, –102.4 and 6.7 for group 1; –12.28, –94.4 and 3.9 for group 2; and –13.16, –99.2 and 6.1 for group 3, respectively.

The mean δ^{18}O, δD and d-excess values for spring water samples (n = 5) were –11.45‰, –89.4‰ and 2.2‰, respectively. The isotopic compositions of spring water samples displayed significant variability in δ^{18}O, δD and d-excess within the group (3.76‰, 24.47‰ and 7.35‰, respectively).

Discussion

Water budget

According to the GW flow model, GW discharge to the river was about 55% from the overall outflow of the model, while 69% from the calculated recharge discharges into the River Kitinen. The mire discharge was about 30 % of the overall outflow and 37% from recharge. The calculated recharge was 80% from the inflow and the remaining 20% was inflow from the model boundaries (Fig. 3). However, these results present only the rectangular model area that does not follow the watershed boundaries, which needs to be taken into account in further water balance calculations.

GW flow patterns

The flow model confirms that the major GW flow direction is towards the River Kitinen, with a minor north-to-south component (Fig. 7), as also seen in the interpolated changes of GW tables (Fig. 10). On the eastern side of the river, the flow direction shifts from east to west towards a NE-to-SW flow in spring. This direction change is related to a more rapid GW table rise in the northern part of the study area. The highest GW table change shifts towards
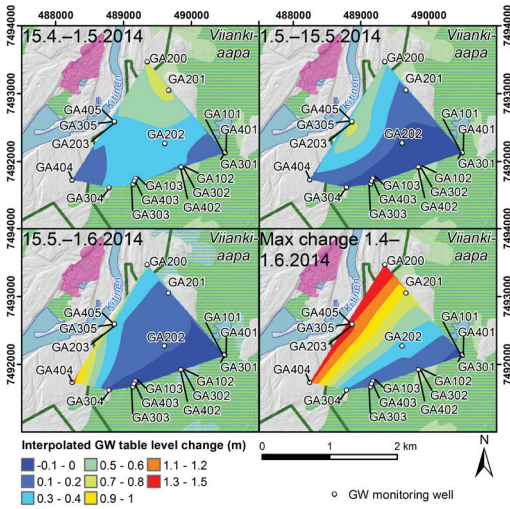
Fig. 10. Natural neighbour interpolated GW table variations from 16 monitoring wells on selected days in the spring of 2014. Terrain elements were reproduced with permission from the copyright owner (National Land Survey of Finland).
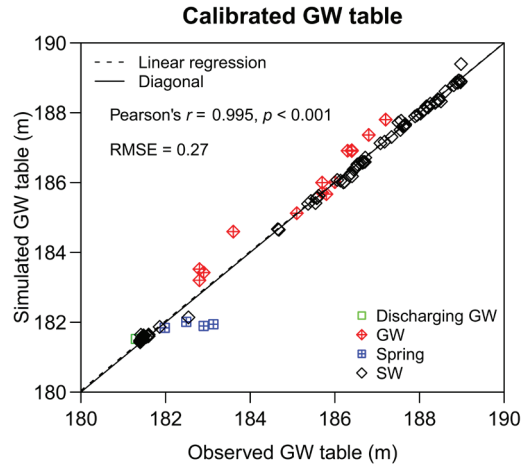

Fig. 11. Observed vs. modelled GW table (see Fig. 7) of the calibrated GW flow model. Linear regression was performed to compare the regressions with the diagonal.

the south during the spring: The maximum change of GW table occurred in wells GA201 and GA200 between mid-April and early May (Fig. 10), and at the end of May, the highest change occurred in the southernmost monitoring well, GA404. The maximum peak in GW table in the well GA404 occurred 24 days after the peak of the well GA201 and 11 days after the peak of the triplet 5 according to cross-correlation indicating slower infiltration or later spring thaw (Figs. 8 and 10).

The annual variation in the GW table appears to indicate that a bank storage setting exists in the eastern bank of the River Kitinen, while GW table variation is most prominent near the river (Figs. 6 and 10). However, the variation of the regulated river stage was estimated to be about 0.5 m, based on the measurements of the Kelukoski and Matarakoski power plants, indicating only a minor effect on GW table variation. The river stage data also indicated that flooding ended after the construction of the Matarakoski and Kelukoski power plants. However, the seven-metre rise of the river stage near the dam raised the altitude of the GW table. Thus, it is possible that water from the River Kitinen flows through the northern part of Kersilönkan-

gas towards Viiankiaapa area (Figs. 1c and 3), which needs to be studied further.

The flanks of the River Kitinen consist of varying braided river and till deposits (Fig. 1), which can form local perched GW conditions due to the high variation in hydraulic conductivities in the bars and channels fills (Lunt *et al.* 2004). Perched GW tables were found in the Kersilönkangas area during field works where perched GW is concealed by an impermeable layer (Appendix Fig. A2, Fig. 1c). Also, multiple springs located at the eastern flank of the River Kitinen are perched, indicating a locally-elevated discharge zone. The high variation of hydraulic conductivities of the sediments and

Table 3. Water budget of the GW flow model of one year presented as cumulative volumes and percentages.

Cumulative volume (m³)	In:		Out:	
Storage	0	0.0%	0	0.0%
Constant head	183 214	8.0%	287 898	12.5%
Drains	0	0.0%	687 842	29.8%
River leakage	5102	0.2%	1 267 768	55.0%
Head dep bounds	267 536	11.6%	60 835	2.6%
Recharge	1 848 461	80.2%	0	0.0%
Total	2 304 313	100.0%	2 304 343	100.0%

existing many separate till layers with lower hydraulic conductivity and perched GW makes the estimation of GW flow patterns challenging, even with flow modelling.

Evaluation of the flow model

The root mean square error (RMSE) of the GW flow model after calibration was 0.27 (Fig. 11) and the correlation of the simulated and observed heads was 0.995. The calculated model bias and mean absolute error (MAE) were –0.03 and 0.15, respectively. The calculated bias and MAE were –0.42 and 0.44 for the automatic monitoring wells and 0.01 and 0.07 for SW points. The calibrated GW flow model overestimated the water level in most of the monitoring wells, probably due to the larger number of SW calibration points, which dominated the results (Fig. 11).

The SW points were derived from LiDAR DEM but the production date was unknown. Thus, flark water levels may indicate a high water table after the spring thaw in some of the data production years from 2008 to 2014. Consequently, the higher water table in the LiDAR DEM points compared to monitoring wells (Fig. 11) probably caused the overestimation of the GW table on the river banks. According to the monitoring wells, the maximum GW variation of the mire area was about 0.3 metres. The flooding commonly occurs in June in aapa mire areas due to the relatively abrupt spring thaw (Solantie 2006). The highest misfits in the calibrated GW flow model were among the spring observations located on the shore of the River Kitinen (Fig. 11). The misfits could be derived from errors in the LiDAR DEM altitude (±20 to ±50 cm RMSE, Hodgson and Bresnahan (2004)), perched springs (Fig. 7) or a structural error in the model. Minor errors in location can easily cause a half-metre error in altitude due to the 20–30° slope of the eastern bank of the River Kitinen.

During the model development, the unit comprising middle sorted deposits was extended to the eastern river bank of the River Kitinen (Fig. 3) compared to the version presented in Åberg A.K. *et al*. (2017a) based on the observed discharge area. Earlier test calibrations indicated

that the peat layer of the Viiankiaapa mire was too thin in the first version of the flow model based on the original 3D geological model described in Åberg A.K. *et al*. (2017a) while the GW table dropped too deep in the western part of the Viiankiaapa mire. The effect of the peat layer thickness was examined with a coarse test GW flow model with a 100-metre resolution, which confirmed the hypothesis that a thicker low *k*-value layer raises the GW table. The thicker peat layer also improved the model results in the calibrated GW flow model. However, some excluded calibration points and the simulated GW depth indicated that the water table was still too low in the mire area approximately 500–1000 m south of Kärväslampi pond in the calibrated GW flow model (Fig. 12). Inspection of *k*-values indicated that an order of magnitude lower hydraulic conductivity of peat catotelm compared to subpeat sediments caused kinks to the GW table on the outer borders of mire leading to a too steep gradient of GW table close to mire border towards the River Kitinen (Fig. 12).

The discharge area can be either located in areas where a lower layer cell has a higher simulated head than a cell above it or to the flooding of cells. The discharge beneath the mire was defined with the negative values of the "flow lower" dataset of MODFLOW, which indicate upward flow (Fig. 12c). Feinstein *et al*. (2012) described GW flooding of the cells in the riparian zone as a simplification of GW discharge. Flooding cells existed on the eastern shore of the river (Fig. 12) and in the mire area in the GW flow model. Flooding may indicate a poor model fit. However, the flooding was mainly present in depressions of the mire area and in the gravel intake area, which are prone to flood during spring. In addition, if a cell is unconfined in the MODFLOW model, it does not take account of the top of the cell or topography (Fig. 12).

MODFLOW-NWT was suitable to run the model without convergence error with its complex geometry and non-linearity due to multiple unconfined (convertible) layers. A major simplification of the model is that below the water table, the model cells are fully saturated and no separation for perched GW was made. However, in reality, GW is not a uniform reservoir within the model area, and it can be partly perched on

top of low permeability layer as observed in field works and in the interpreted GPR profiles. In a transient MODFLOW model, a perched GW table can be modelled with the presentation of the impermeable layer as inactive cells, as in a quasi 3D model (e.g. Weiss and Gvirtzman (2007)), and by using the recharge package or the unsaturated zone flow (UZF) extension. However, the accuracy of the *k*-value estimations and the distribution of till units remained uncertain due to highly variable hydraulic conductivities and the mixing of sediments during the drilling, which was observed during the grain-size analysis. In addition, the impermeable layer approach was not applicable to scattered units. The hydraulic conductivity measurements indicated high heterogeneity in sediments. In addition, the *k*-value variation of the eastern and western sides of the river, especially in the case of the lower till deposits, is so considerable that they may not represent the same geological unit as presented in the 3D geological model. Furthermore, the simplification of the material of the fractures and the faults as uniform hydraulic conductivity zones could be an oversimplification in the model. Faults and fractures can considerably affect the flow patterns (see e.g., Bense *et al*. 2003) depending on whether the faults or fractures have higher or lower hydraulic conductivity than their surroundings. The hydraulic conductivity of the fractures and faults can be highly variable depending on the material of the fracture filling, the fluid chemistry, and weathering of the bedrock, and it can change as time passes (Stober and Bucher 2015). The nature of weathering is also important since chemically weathered clay material can fill the voids and create low conductivity barriers. Also, according to Hall (1986), fresh bedrock may be present within the weathered units, which can make the hydraulic connections between bedrock and surface sediment complex. However, deep weathered troughs with thick weathered and fractured bedrock zone occur where faults intersect. These depressions, based on preliminary observations, appear to be associated with an increased clay saprolite fraction and lower permeability weathered bedrock material (SRK 2019, unpubl. data). As the estimated bedrock *k*-values are relatively high especially in the western part of the Viianki-
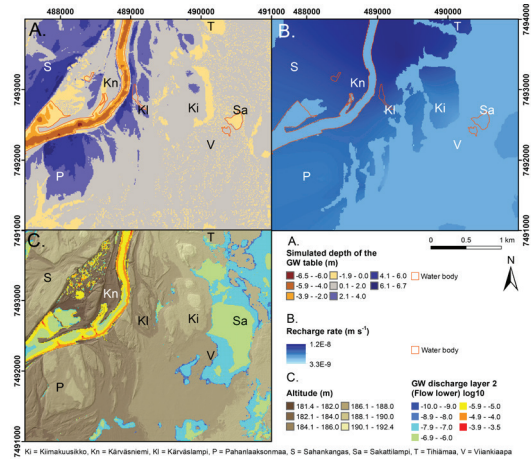

Fig. 12. A: Simulated GW table depth. Negative values indicate flooding cells. **B**: Estimated recharge rate. **C**: The simulated upward flow of the GW in the bottom of layer 2 derived from flow lower dataset of cell budget file of MODFLOW indicating discharge from subpeat sediments in the mire area. The flooding of GW by the river indicates discharge into the river. In unconfined cells, only the bottom of the cell is used to calculate the water table (Harbaugh 2005) and the top is assumed to be infinite. LiDAR DEM was modified and reproduced with permission from the copyright owner (National Land Survey of Finland). Water bodies were reproduced with permission from the copyright owner (National Land Survey of Finland).

aapa mire, it is likely that more GW exists in fractured/weathered part of bedrock unit/zone than in the sorted sediments of the riverbank in the study area. However, the measurement from open drill holes can represent either the average hydraulic conductivity or the hydraulic conductivity of a single fracture, which need to be taken into consideration. Since the bedrock *k*-value was earlier found to be sensitive to model results, further understanding of the thickness and the properties of the upper fractured/weathered zone is needed.

During the model development, the HK, RIV, RCH and DRN parameters were tested with a sensitivity analysis using the open source code, *UCODE_2014* (Hill and Tiedeman 2007, Poeter *et al*. 2014) with the ModelMate GUI (Banta 2011) to detect which parameters are sensitive enough to be estimated with automated parameter estimation. The sensitivity analysis and calibration test results indicated that the RIV and the DRN conductance had low sensitivity close to 0.01 times the highest sensitivity occurring

in bedrock *k*-value when it was originally tested with one homogenous parameter zone, which made parameters estimation difficult (see Hill 1998). Using many parameters in a GW flow model commonly causes parameter insensitivity and correlation in parameter estimation (Feinstein *et al.* 2012), causing non-convergences in the automatic parameter estimation. In the later version of the model, the HK parameters except for the bedrock fractures and faults were first manually defined based on the *k*-value measurements to represent the geological variability. Then, automatic parameter estimation was used for RIV and DRN conductance and the bedrock fractures and faults. Precise calibration of the model is not probably possible with this type of model due to the existing perched GW tables and uncertainty over the sedimentary structure. However, parameter estimation with pilot points using PEST (Doherty 2003) could improve the calibration. In addition, the model does not calculate runoff or unsaturated zone processes, which may cause misinterpretations of the recharge rates. An alternative approach to reinforce the calibration is to set a higher uncertainty level for mire area points compared to observation wells. Thus, to obtain more sophisticated model results, the use of models including the full hydrological cycle, such as ParFlow (Kollet and Maxwell 2006) or Arctic Terrestrial Simulator (ATS) (Coon *et al.* 2013), would be suggested for more detailed modelling of the hydrological settings of the study area.

GW recharge

Recharge is the most difficult parameter to estimate (Anderson and Woessner 1992). Only a few recharge estimations exist near our study site. According to Hyyppä (1962), GW recharge in sandy areas in central Lapland is about 42–61% of the rainfall. He noticed that during winter, the GW table drop was constant in deposits having a high hydraulic conductivity, while low hydraulic conductivity areas have more diverse GW tables. However, during the snow-cover period, recharge is blocked and existing GW slowly flows away from aquifers (Kuusisto 1984). The estimated recharge rate of 10–69% in this study

is close to Hyyppä's estimation. However, the recharge rate strongly depends on the geology of the local systems. The estimated recharge rate in the Viiankiaapa mire area was 19% from precipitation, which falls within the observed values of 3–20% in a fen area with sandy bottom sediments in Alaska (Siegel 1988). In addition, the GW wells indicated that the subpeat sediments gain water during spring flood (Fig. 8). The recharge in the mire seemed to occur in the cells that were higher such as peat mounds as observed by Reeve *et al.* (2000) meaning the topography controls the recharge/discharge pattern in the mire. The assumption that the recharge rate is directly proportional to precipitation is an oversimplification. It ignores the changes in evaporation and runoff rates.

The statistically significant cross-correlation of the SWE with GW table fluctuation, with a significance of 0.062 ($n = 1041$), indicated that the main recharge period occurred from April to May in 2012–2015 during spring thaw water. The lag between the SWE and GW table peak varied from 6–140 days (Fig. 4) and the GW table peak occurred about 30–60 days after the SWE peak (Fig. 8). The cross-correlation appeared to overestimate the lag in some wells due to the inverted shape of the GW table curves compared to the SWE (Fig. 8). The fluctuations of the GW table in the mire area were minor, indicating lower recharge rates and the response to snowmelt more rapid and earlier than near the river banks, which indicate shorter infiltration time and earlier thaw.

Cross-correlation analysis indicated that rainfall caused a rapid rise in the GW table in almost all monitoring wells during summer and autumn (Fig. 4) that usually lasted less than two weeks (Fig. 8). The cross-correlation (0.07–0.16) lag between precipitation and the GW table fluctuation was 1–2 days in monitoring wells GA201, GA200, GA304, GA102 and GA202, 8–9 days in GA203 and GA405 and 0 days in GA404 with a significance of 0.0505 ($n = 1568$) (Fig. 4). The cross-correlation of GA302 and GA301 failed, but closer inspection of the data (Fig. 8) hinted that the GW table rise was related to the intensity of the precipitation. Rainfall-influenced GW table elevations lasted longer in autumns than in summers, probably

due to the longer and more intense rainfall seasons.

The flow modelling results indicated downward flow of the GW (recharge area) in the eastern bank of the river, as seen in triplet 5 and triplet 3 wells (Appendix Fig. A2), which had the lowest head in the deepest well. The wells of triplet 1 (Appendix Fig. A2) indicate discharge within the mire area according to model results and considering that the deeper wells have the highest head, while triplet 2 indicated recharge both in model results and observations. Altogether, the model overestimated the water tables in all of the triplets, and the simulated head differences in the wells with different depths were minor compared to the observed values. Overall, the area from Pahanlaaksonmaa to Kärväslampi, the Sahankangas area and the Sakattikumpu areas can be considered as recharge areas. Other likely recharge areas outside the model area include Särkikoskenmaa (Appendix Fig. A2), which is mostly covered by sand dunes, and Viiankiaavan Petäjäsaari (Appendix Fig. A2), which is also covered by sandy and gravelly deposits (Fig. 1b).

GW discharge

The modelling results indicated that upward GW flow (discharge) exists within the mire area and most abundantly along the shores of Kitinen (Fig. 12). The UAV-TIR survey identified GW discharge on the eastern side of the River Kitinen, supporting the results of the GW flow model. TIR imagery receives thermal radiation emitted from the "skin" layer (< 0.1 mm), and only GW contributions reaching the surface of the soil or water bodies can, therefore, be detected (Torgersen *et al.* 2001). TIR imagery can be biased by thermal stratification in water bodies if the stratified conditions are not recognized (Torgersen *et al.* 2001, Rautio *et al.* 2015). While the UAV-TIR survey indicates only GW discharge that reaches the water surface the modelling gives estimates to the discharge rate. However, due to the poorly known bottom sediments of the River Kitinen, it is hard to evaluate the exact extent of the discharge areas in the river bottom. Interestingly, the fractures of bedrock

seem to affect the river discharge which needs to be studied further (Fig. 12).

Classification of the GW recharge and discharge areas of mires is complicated (Laitinen *et al.* 2007). Peat usually has a low hydraulic conductivity and aquitard-like properties. The total flow pattern of mires cannot be observed from the surface or acrotelmic flow, because vertical flow may also occur in the peat (Laitinen *et al.* 2007). The loss of water due to evaporation in a patterned fen can be close to the potential evaporation (Price *et al.* 1991). According to (Reeve *et al.* 2000) recharge/discharge pattern of a fen is controlled by the topography and properties of the subpeat sediment. When the subpeat sediment has a low *k*-value, the water movement is more horizontal. Instead, a high *k*-value adds a vertical component in flow, and water exchange from sediments beneath the mire also occurs. Sorted sandy sediments that underlie the peat layer of the Viiankiaapa mire forms a more or less continuous layer that can provide GW discharge into the mire. However, the upward flow in the mire area was only slight in the model due to the low hydraulic conductivity of the peat unit (Appendix Fig. A3). The topography of the Viiankiaapa mire seemed to affect the GW recharge/discharge pattern according to model

Table 4. Cross-correlation results for SWE vs. GW table and precipitation vs. GW table. Lags of between 29-66 days represent the most realistic values in the SWE vs. GW table results (see Fig. 8).

Well	SWE & GW table		Precip. & GW table	
	Lag[1]	CC[2]	Lag[1]	CC[2]
GA102	54	0.30	—	0.11
GA200	129	0.56	1	0.15
GA201	122	0.42	1	0.16
GA202	66	0.37	1	0.09
GA203	140	0.46	9	0.13
GA301	6	0.72	—	0.06
GA302	49	0.47	—	0.04
GA304	52	0.38	1	0.10
GA403	29	0.27	—	0.07
GA404	131	0.57	0	0.15
GA405	140	0.46	8	0.13

[1]Lag unit is days
[2]Cross-correlation coefficient (dimensionless)

results as local topographic lows were more discharge and topographical elevations more recharge dominated. Discharge from the subpeat sediments occurred mainly in the middle of mire while other areas were dominated by recharge. In addition, heterogeneity in hydraulic conductivity can vary considerably in peatland, as observed in previous studies (Fraser *et al.* 2001, Ferlatte *et al.* 2015), which should be taken into account in the future GW flow model.

Using DRN for GW discharge in the mire was a straightforward method since discharge occurs when the simulated head is slightly above the topography. However, DRN oversimplifies the process since it does not take into account surface water flow physics and the calculations based on Darcy's equation that is suited for non-laminar porous flow. Another challenge is that according to Batelaan and De Smedt (1998), the GW discharge locations should be known prior to the modelling and use DRN only in those locations. Discharge areas could be observed as cold anomalies. The georeferenced TIR data provide highly detailed thermal information and appear to be applicable in spatial analysis (Fig. 9b). However, the areal coverage was extremely small, and it is, therefore, necessary to prioritize the imagery targets. Nevertheless, the DRN is usable for an initial guess of discharge locations in a large scale model as it locates the upwelling, and therefore, it can be used for targeting a UAV-TIR survey. Then the UAV-TIR survey could be applicable to verify the modelled GW discharge areas of the mire on a more detailed scale. Moreover, TIR imagery is sensitive to the prevailing weather conditions and variability in these conditions during the TIR survey. Clear cloudless weather conditions develop strong shadows that increase the time needed in post-processing, as shadow-induced anomalies need to be removed from GW-induced anomalies.

Heterogenic origin of GW

According to Clark and Fritz (1997), the isotopic composition of shallow GW does not significantly deviate from the mean weighted annual composition of precipitation in temperate cli-

mates. The isotope composition of shallow GW follows the local meteoric water line (LMWL) in Finland (Kortelainen and Karhu 2004). The measured mean $\delta^{18}O$, δD and d-excess values of all GW observation well water samples (–13.11‰, –99.1‰ and 5.7‰; $n = 21$) differed overall from the previously reported values of Kortelainen (2007) for natural GW (mean –14.68‰, –107.8‰ and 10.1‰) in Siurunmaa, Sodankylä, located 11 km south of the study area (Fig. 1b) during a 4-year monitoring period from 2001 to 2004.

The considerable variability in the stable isotope composition of GW observation wells appears to be connected to the landform types: open mire, forested areas and banks of the river. The measured $\delta^{18}O$, δD and d-excess values of GW observation wells ($n = 6$) in open wet mire areas have evaporated isotope values (–12.28‰, –94.4‰ and 3.9‰, respectively) compared to previously reported stable isotope composition of GW close to study area (Kortelainen 2007). Generally, d-excess values significantly below 10‰ represent waters influenced by evaporation (Brooks *et al.* 2012). The stable isotope values of GW in wetlands containing standing water cannot be considered un-fractioned due to GW recharge from evaporated SWs (Hunt *et al.* 1996). Therefore, GW in wet mire areas has an evaporated component compared to GW formed directly from precipitation immediately after infiltration. Kellner (2001) observed that open water areas are dominated by evaporation and areas of extensive vascular vegetation tend to be dominated by transpiration. In the Viiankiaapa mire, both open water and vascular vegetation areas are common, leading to difficulties in estimating the transpiration and evaporation proportions. According to Ferlatte *et al.* (2015), vertical connections between mires and underlying aquifers appear to be very common. Therefore, the GW samples with evaporated $\delta^{18}O$, δD and d-excess values could indicate an evaporated source water component.

The GW observation wells located in forested areas have measured mean $\delta^{18}O$, δD and d-excess values closest to the previously reported values of Kortelainen (2007) for GW in the study area. Two GW observation wells (GA100, GA200) have evaporated values dif-

fering from the other wells in forested areas. Observation well GA100 was installed in the peat layer and should be considered more as a SW monitoring well than a true GW observation well that can be noticed as a negative *d*-excess value of –1.59‰. Observation well GA200 is located in a forested area but has an evaporated isotope composition (–12.74‰, –98.05‰ and 3.87‰), indicating an influence of SW. GW level in the observation well GA200 is close to the ground surface meaning, a short retention time of SW infiltrating into the aquifer and could, therefore, explain the observed evaporated isotope composition. If these two GW observation wells are excluded, the mean δ^{18}O, δD and *d*-excess values for the GW observation wells in forested areas are –14.24‰, –105.65‰ and 8.27‰, respectively, which agrees closely with the study of Kortelainen (2007).

The stable isotope composition of GW observation wells in the proximity of the River Kitinen (*n* = 6) is more variable compared to stable isotope composition of GW observation wells at forested areas and open mire areas. (Appendix Table A4). All six samples were affected by evaporation based on both enriched δ^{18}O and δD, as well as evaporated *d*-excess values (Fig. 9 and Appendix Table A4). Therefore, it is possible that all of these wells are affected by the short respond to precipitation recharge due to the highly conductive sand and gravel deposits around the periphery of mire, the River Kitinen or GW recharges from evaporated water from peatland, but the evaporated water source is not definable based on stable isotope composition.

The River Kitinen samples are slightly dislocated from the LMWL (Fig. 9b) and the *d*-excess values indicated evaporation effects (Appendix Table A4, Fig. 13). Interestingly, the measured δ^{18}O, δD and *d*-excess values of GA405 (–12.50‰, –96.2‰ and 3.8‰, respectively) in triplet 5 indicated a SW effect in the deepest observation well drilled into the bedrock (Fig. 14), but the SW source cannot be identified based on stable isotope composition. Further tracers will be needed to identify the source of the evaporated water in GA405.

All spring water samples (*n* = 5) were affected by evaporation based on both enriched
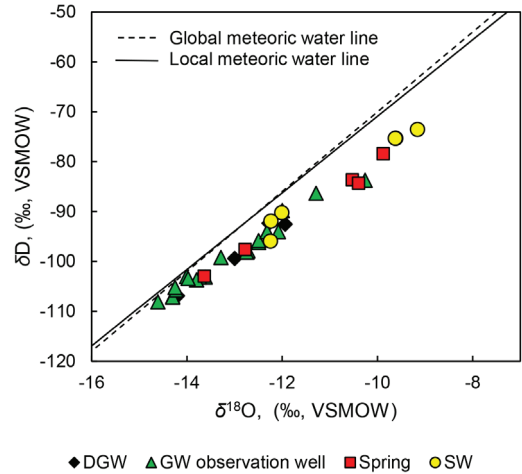

Fig. 13. The relationship between δD and δ^{18}O in GW and SW of the study area. The local meteoric water line (solid line) (δD = 7.67 δ^{18}O + 5.79‰ (Kortelainen 2007)) and global meteoric water line (dashed line) (δD = 8 δ^{18}O + 10‰ (Craig (1961)) are shown as lines for comparison.
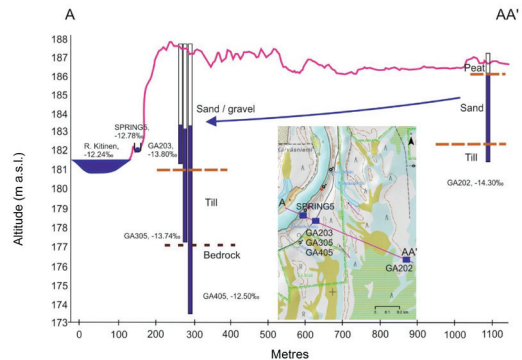

Fig. 14. Schematic figure of the GW flow direction and triplet 5 wells in the Tuulivuopaja area, 200 m south of Kärväslampi (see Fig. 9). Base map was reproduced with permission from the copyright owner (National Land Survey of Finland).

δ^{18}O and δD, as well as evaporated *d*-excess values (mean –11.45‰, –89.4‰ and 2.2‰, respectively) (Fig. 9 and Appendix Table. 4). The stable isotope composition of spring waters was variable and overall differed from the previously reported values of Kortelainen (2007) for natural GW in the proximity of the study area. The most evaporated spring water samples (SPRING7, SPRING6 and SPRING4) were
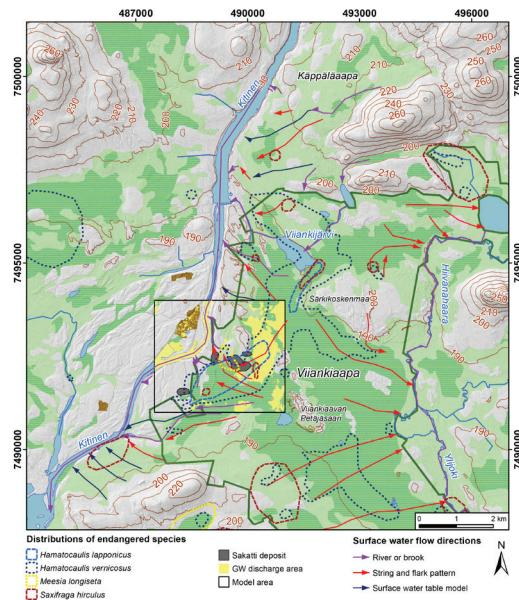
Fig. 15. Comparison of the distribution of GW-dependent endangered plant species with SW flow directions and GW discharge. The major habitats of the species are within the model area and on the southern side of Viiankijärvi. The Sakatti deposit is modified after Brownscombe et al. (2015). Terrain elements were reproduced with permission from the copyright owner (National Land Survey of Finland). Distributions of endangered species modified after the Hertta information systems of the Finnish Environment Institute (23 Sep. 2015), reproduced with permission from the copyright owner.

taken from the Kärväslampi area and from the proximity of Ruosteoja (Fig. 4). In the proximity of Kärväslampi pond, only a narrow ridge consisting of coarse-grained sediments is situated between the sampled springs and Kärväslampi pond. Therefore, these spring water samples could be composed of Kärväslampi pond water, the precipitation recharge and surface waters from the mire that have infiltrated through the sediments. The spring sample close to Ruosteoja could be re-infiltrated mire water. According to Åberg A.K. *et al.* (2017a), the sedimentary units are very heterogeneous and hydraulically poorly connected, representing different GW systems, which could explain the spatially variable isotope composition of springs.

Generally, the variable origins of GW in the open mire, forested areas and river-influenced sediments can be observed as the heterogeneous

stable isotope composition of GW and springs. Heterogeneous stable isotope composition of GW and spring water indicate that aquifers are not connected but they are dispersed and compartmentalised and their areal coverage is limited. One would assume more uniform stable isotope composition if there were a well-connected and extensive sedimentary aquifer in the study area.

GW and SW flow patterns and distribution of endangered species

The occurrence of *Hamatocaulis vernicosus* and *H. lapponicus* reflects GW seepage into the mire (Ulvinen 2009, Ulvinen and Sallantaus 2009). The flow modelling results indicating upward flow from subpeat sediments are consistent with this scenario (Fig. 12). However, the model appears to underestimate the area of the discharge zone compared to the distribution of the GW-dependent *H. vernicosus* (Fig. 15). The densest occurrence of *Saxifraga hirculus* is only located on the southern side of Sakattilampi, where the GW table variations are minor (less than one metre). It has been noted that nutrient-rich bedrock makes the occurrences of eutrophic fens more common in central Lapland than in other areas of Finland (Kaakinen *et al.* 2008). Thus, the occurrence of fen patches could be linked to the ultramafic bedrock exposures close to the Sakatti deposit (see Brownscombe *et al.* (2015) Fig. 3.7.3). On the other hand, the occurrences may be related to old river channels in the subpeat sediments. The densest distribution of *Meesia longiseta* exists near the outcrops of the deposit (Fig. 15). *Hamatocaulis lapponicus*, *H. vernicosus* and *Saxifraga hirculus* usually exist in iron-rich fens (Sallantaus 2006), indicating anoxic conditions. The distribution of these three species also followed the SW and GW flow directions from NE towards SW in the Viiankiaapa mire (Fig. 15), which may indicate a nutrient source close to the watershed about one kilometre south of the Viiankijärvi lake (Fig. 15). For a better understanding of the possible connection between the distributions of plants and ultramafic rocks, the bedrock of the study area needs to be further investigated.

Conclusions

GW flow modelling was found to be useful for defining the spatial location and a general picture of the rates of GW discharge and recharge. Whereas, The WTF and EMR methods utilized for GW monitoring well data give more precise information of GW recharge rates and relations of SWE and precipitations variations to GW recharge. TIR is suitable methods for localizing GW discharge area in a detailed matter. Isotopes indicate GW/SW interaction and their ratios bringing detailed information of GW origin.

The results of this study indicate that GW mainly flows towards the River Kitinen. On the eastern side of the river, GW flows from east to west, gradually changing its flow pattern towards a more NE–SW direction during the spring thaw. Variations in the GW table were dependent on the spring thaw and the higher recharge rate in the northern part of the river bank in the model area. The higher variation in the northern part may indicate higher recharge or the influence of the Matarakoski dam on the GW table during the higher river stage. However, confirmation of this requires expansion of the model area in the future to the north.

Recharge within the mire was related to peat mounds on the topography while discharge was more common in the topographic lows. Overall the slope of the GW table was too steep compared the observations due to a local possibly perched setting in the river banks. The distribution of the dense till with low conductivity should be better understood to evaluate the distribution of the perched system.

The hydrostratigraphy of the study area is complex, with varying hydraulic properties of tills, intertill sorted sediment layers and discontinuous subtill deposits considerably affecting the modelled GW tables and flow patterns. In addition, bedrock fractures and faults can affect locally to the flow patterns and the GW table, and their hydraulic properties need to be studied further for understanding the connections of bedrock aquifers and surficial aquifers. The uncertainties in the 3D sedimentary model reflect uncertainties in the flow model. On the other hand, the flow model can be used to evaluate and improve the 3D model. Complex hydrostratigraphy is also reflected in the variability of stable isotope composition observed in the GW and springs. The stable isotope composition of springs, in situ temperature measurements and the UAV-TIR survey identified GW discharge on the eastern shoreline of the River Kitinen and therefore supported the GW flow model.

The flow modelling indicated upward flow in the central area of the mire. However, the distribution of the modelled discharge zone was probably underestimated compared to the distribution of GDEs. UAV-TIR indicated GW discharge on the outer fringe of the mire and it is an applicable method for verification of the modelled GW discharge areas in the mire in the future. It is possible that SW/GW flow patterns and their annual fluctuations have an influence on the GDEs of the mire, and their distribution could be used for further model development. In addition, the stable isotope composition indicated that mire water might be at least partly re-percolated and that SW influenced water discharges to the springs in the banks of the river. Furthermore, SW-influenced water was found in a shallow bedrock well. Consequently, the flow modelling and the stable isotopic composition shows that the heterogeneity of the fractured bedrock and peat unit should be taken into more detailed consideration in future modelling to improve our understanding of the water balance and hydraulic connections of water resources in planning activities of the mining site development. The results will be used as part of the baseline study of the mining development site and in the environmental impact assessment of the Sakatti project (http://www.ymparisto.fi/sakatinkaivosYVA [In Finnish]).

References

Aalto A. 2008. Vesivoiman lisärakentamisen tarve ja mahdollisuudet Suomessa. *Vesitalous* 2: 8–11.

Åberg A.K., Salonen V.-P., Korkka-Niemi K., Rautio A., Koivisto E. & Åberg S.C. 2017a. GIS-based 3D sedimentary model for visualizing complex glacial deposition in Kersilö, Finnish Lapland. *Boreal Environment Research* 22: 277–298.

Åberg S.C., Åberg A.K., Korkka-Niemi K. & Salonen V.-P. 2017b. Hydrostratigraphy and 3D Modelling of a Bank Storage Affected Aquifer in a mineral exploration area in Sodankylä, Northern Finland. *Mine Water & Circular Economy* 1: 237–244.

Alanne M., Honka A. & Karjalainen N. 2014. *Lokan ja Porttipahdan tekojärvien säännöstelyn kehittäminen; Yhteenveto ja toimenpidesuositukset.* Lapin ELY-keskus, available at http://www.doria.fi/handle/10024/98875.

Anderson M.P. 2005. Heat as a Ground Water Tracer. *Groundwater* 43: 951–968.

Anderson M.P. & Woessner W.W. 1992. *Applied groundwater modeling: simulation of flow and advective transport.* Academic Press, San Diego, CA.

Banta E.R. 2011. *ModelMate — A Graphical User Interface for Model Analysis: U.S. Geological Survey Techniques and Methods.* U.S. Geological Survey Techniques and Methods 6–E4, available at http://water.usgs.gov/software/ModelMate/.

Barthel R. & Banzhaf S. 2016. Groundwater and Surface Water Interaction at the Regional-scale – A Review with Focus on Regional Integrated Models. *Water Resources Management* 30: 1–32.

Batelaan O. & De Smedt F. 1998. An adapted DRAIN package for seepage problems. In: *MODFLOW'98 Proceedings*, Citeseer, pp. 555–562.

Bense V.F., Van Balen R.T. & De Vries J.J. 2003. The impact of faults on the hydrogeological conditions in the Roer Valley Rift System: an overview. *Netherlands Journal of Geosciences* 82: 41–54.

Bouwer H. & Rice R.C. 1976. A slug test for determining hydraulic conductivity of unconfined aquifers with completely or partially penetrating wells. *Water Resources Research* 12: 423–428.

Brooks J.R., Wigington Jr P.J., Phillips D.L., Comeleo R. & Coulombe R. 2012. Willamette River Basin surface water isoscape (δ^{18}O and δ^2H): temporal changes of source water within the river *Ecosphere* 3: 1–21.

Brownscombe W., Ihlenfeld C., Coppard J., Hartshorne C., Klatt S., Siikaluoma J.K. & Herrington R.J. 2015. Chapter 3.7 — The Sakatti Cu-Ni-PGE Sulfide Deposit in Northern Finland. In: O'Brien W.D.M.L. (ed.), *Mineral Deposits of Finland*, Elsevier, pp. 211–252.

Clark I. & Fritz P. 1997. *Environmental Isotopes in Hydrogeology.* CRC, New York.

Clay A., Bradley C., Gerrard A.J. & Leng M.J. 2004. Using stable isotopes of water to infer wetland hydrological dynamics. *Hydrol. Earth Syst. Sci.* 8: 1164–1173.

Coon E., Berndt M., Garimella R., Moulton J., Manzini G. & Painter S. 2013. Computational advances in the Arctic terrestrial simulator: modeling permafrost degradation in a warming Arctic. In: *AGU Fall Meeting Abstracts*.

Craig H. 1961. Isotopic variations in meteoric waters. *Science* 133: 1702–1703.

Dansgaard W. 1964. Stable isotopes in precipitation. *Tellus* 16: 436–468.

Doherty J. 2003. Ground water model calibration using pilot points and regularization. *Groundwater* 41: 170–177.

Doherty J. 2015. *Calibration and uncertainty analysis for complex environmental models.* Watermark Numerical Computing.

Dugdale S.J., Bergeron N.E. & St-Hilaire A. 2013. Temporal variability of thermal refuges and water temperature patterns in an Atlantic salmon river. *Remote Sensing of Environment* 136: 358–373.

Eilu P. 2012. *Mineral deposits and metallogeny of Fennoscandia.* Geological Survey of Finland, Espoo, Special Papers 53.

Eurola S. & Huttunen A. 2006. Mire plant species and their ecology in Finland. In: Lindholm T. & Heikkilä R. (eds.), *Finland–land of mires Finnish Environment Institute*, Oulu, pp. 127–144.

Feinstein D.T., Fienen M.N., Kennedy J.L., Buchwald C.A. & Greenwood M.M. 2012. *Development and Application of a Groundwater/Surface-Water Flow Model using MODFLOW-NWT for the Upper Fox River Basin, Southeastern Wisconsin.* U.S. Geological Survey Scientific Investigations Report 2012–5108, Wisconsin, available at http://pubs.er.usgs.gov/publication/sir20125108.

Ferlatte M., Quillet A., Larocque M., Cloutier V., Pellerin S. & Paniconi C. 2015. Aquifer–peatland connectivity in southern Quebec (Canada). *Hydrological Processes* 29: 2600–2612.

Fleckenstein J.H., Krause S., Hannah D.M. & Boano F. 2010. Groundwater-surface water interactions: New methods and models to improve understanding of processes and dynamics. *Advances in Water Resources* 33: 1291–1295.

Foster D.R., King G.A., Glaser P.H. & Wright H.E., Jr. 1983. Origin of string patterns in boreal peatlands. *Nature* (London) 306: 256–258.

Fraser C.J.D., Roulet N.T. & Lafleur M. 2001. Groundwater flow patterns in a large peatland. *Journal of Hydrology* 246: 142–154.

Gat J.R. & Gonfiantini R. 1981. *Stable isotope hydrology Deuterium and oxygen-18 in the water cycle.* Series no. 210, IAEA, International Atomic Energy Agency (IAEA).

Hall A.M. 1986. Deep weathering patterns in north-east Scotland and their geomorphological significance. *Zeitschrift fur Geomorphologie* 30: 407–422.

Hall A.M., Sarala P. & Ebert K. 2015. Late Cenozoic deep weathering patterns on the Fennoscandian shield in northern Finland: A window on ice sheet bed conditions at the onset of Northern Hemisphere glaciation. *Geomorphology* 246: 472–488.

Hänninen P., Lintinen P. & Sutinen R. 2000. Suomen maaperän vedenjohtavuus. *Vesitalous* 6: 16–19.

Harbaugh A.W. 2005. *MODFLOW-2005, the US Geological Survey modular ground-water model: the ground-water flow process*. US Department of the Interior, US Geological Survey Reston, VA.

Hill M.C. 1998. *Methods and guidelines for effective model calibration; with application to UCODE, a computer code for universal inverse modeling, and MODFLOWP, a computer code for inverse modeling with MODFLOW*. Water-Resources Investigations Report 98-4005, available at http://pubs.er.usgs.gov/publication/wri984005.

Hill M.C. & Tiedeman C.R. 2007. *Effective groundwater model calibration: with analysis of data, sensitivities, predictions, and uncertainty*. John Wiley & Sons.

Hirvas H. 1991. Pleistocene stratigraphy of Finnish Lapland. *Bulletin — Geological Survey of Finland* 354: 123 pp.

Hjelt A. & Pääkkö E. 2006. Viiankiaavan hoito- ja käyttösuunnitelma. *Metsähallituksen luonnonsuojelujulkaisuja. Sarja C* 11: 51.

Hodgson M.E. & Bresnahan P. 2004. Accuracy of airborne LiDAR-derived elevation. Photogrammetric *Engineering & Remote Sensing* 70: 331–339.

Hughes J.D. & Liu J. 2008. MIKE SHE: Software for Integrated Surface Water/Ground Water Modeling. *Groundwater* 46: 797–802.

Hunt R.J., Krabbenhoft D.P. & Anderson M.P. 1996. Groundwater Inflow Measurements in Wetland Systems. *Water Resources Research* 32: 495–507.

Hunt R.J., Bullen T.D., Krabbenhoft D.P. & Kendall C. 1998. Using Stable Isotopes of Water and Strontium to Investigate the Hydrology of a Natural and a Constructed Wetland. *Groundwater* 36: 434–443.

Huokuna M. 1991. Jokijäätutkimusprojektin havainnot. *Vesi- ja ympäristöhallituksen monistesarja* Nro 300: 43 pp. 47 Appendices.

Hvorslev M.J. 1951. Time lag and soil permeability in ground-water observations. *Bull. No. 36, Waterways Exper. Sta. Corps of Engrs, U.S. Army, Vicksburg, Mississippi*: pp. 1–50.

Hyyppä J. 1962. *Pohjavesitutkimuksia Sodankylän pitäjän pohjoisosaan suunnitellun Lokan patoamisaltaan ympäristössä*. Geologian tutkimuskeskus, Maaperäosasto, available at http://tupa.gtk.fi/raportti/arkisto/p13_5_3_037.pdf.

Johansson P. & Kujansuu R. 2005. *Pohjois-Suomen maaperä: maaperäkarttojen 1:400 000 selitys*. Summary: Quaternary deposits of Northern Finland - Explanation to the maps of Quaternary deposits 1:400 000. Erikoisjulkaisut — Special Publications, Geologian tutkimuskeskus, Espoo.

Johnson A.I. 1967. *Specific yield: compilation of specific yields for various materials*. Water Supply Paper, Washington, D.C., available at http://pubs.er.usgs.gov/publication/wsp1662D.

Kaakinen E., Aapala K. & Kokko A. 2008. Suoluonnon monimuotoisuus. In: Korhonen R., Korpela L.& Sarkkola S. (eds.), *Suomi-Suomaa. Soiden ja turpeen tutkimus ja kestävä käyttö (eng.Finland-Land of mires. Mire and peat research and sustainable use)*. Finnish Peatland Society, pp. 36–37.

Karplund T. 1990. *Sodankylän ympäristönhoito-ohjelma*. Nordia tiedonantoja, Pohjois-Suomen maantieteellinen seura r.y., Oulu, 90 p.

Kauppi S., Mannio J., Hellsten S., Nysten T., Jouttijärvi T., Huttunen M., Ekholm P., Tuominen S., Porvari P. & Karjalainen A. 2013. *Arvio Talvivaaran kaivoksen kipsisakka-altaan vuodon haitoista ja riskeistä vesiympäristölle*. Suomen ympäristökeskuksen raportteja 11, available at http://hdl.handle.net/10138/38465.

Kellner E. 2001. Surface energy fluxes and control of evapotranspiration from a Swedish Sphagnum mire. *Agricultural and Forest Meteorology* 110: 101–123.

Kendall C. & Coplen T.B. 2001. Distribution of oxygen-18 and deuterium in river waters across the United States. *Hydrological Processes* 15: 1363–1393.

Kollet S.J. & Maxwell R.M. 2006. Integrated surface–groundwater flow modeling: A free-surface overland flow boundary condition in a parallel groundwater flow model. *Advances in Water Resources* 29: 945–958.

Korhonen J. 2007. Suomen vesistöjen virtaaman ja vedenkorkeuden vaihtelut. *Suomen ympäristö* 45: 120 pp.

Kortelainen N. 2007. *Isotopic fingerprints in surficial waters : Stable isotope methods applied in hydrogeological studies*. PhD Thesis, University of Helsinki.

Kortelainen N. & Karhu J.A. 2004. Regional and seasonal trends in the oxygen and hydrogen isotope ratios of Finnish groundwaters: a key for mean annual precipitation. *Journal of Hydrology* 285: 143–157.

Krabbenhoft D.P., Bowser C.J., Anderson M.P. & Valley J.W. 1990. Estimating groundwater exchange with lakes: 1. The stable isotope mass balance method. *Water Resources Research* 26: 2445–2453.

Kujansuu R. 1967. On the deglaciation of western Finnish Lapland. Bulletin de la Commission Geologique de Finlande 232: 98 pp.

Kulmala P. 2005. Lettorikon tila Suomessa. *Metsähallituksen luonnonsuojelujulkaisuja, Sarja A* 148: 71 pp.

Kuusisto E. 1984. Snow accumulation and snowmelt in Finland. V*esientutkimuslaitoksen julkaisuja* 55: 149 pp.

Lahermo P. 1970. Chemical geology of ground and surface waters in Finnish Lapland. *Geological Survey of Finland, Bulletin — Bulletin de la Commission Géologique de Finlande* 242: 106 p.

Lahermo P. 1973. The ground water of Central and West Lapland interpreted on the basis of black and white aerial photographs. *Geological Survey of Finland, Bulletin — Bulletin de la Commission Géologique de Finlande* 262: 5–48.

Laitinen J., Rehell S. & Huttunen A. 2005. Vegetation-related hydrotopographic and hydrologic classification for aapa mires (Hirvisuo, Finland). *Annales Botanici Fennici* Vol. 42, No. 2: 107–121.

Laitinen J., Rehell S., Huttunen A., Tahvanainen T., Heikkila R. & Lindholm T. 2007. Mire systems in Finland; special view to aapa mires and their water-flow pattern. *Suo* 58: 1–26.

Lappalainen E. 1970. Über die spätquartäre Entwicklung der Flussufermoore Mittel-Lapplands. *Bulletin de la Commission Geologique de Finlande* No. 244: 79 pp.

Lee D.R. & Cherry J.A. 1979. A Field Exercise on Ground-water Flow Using Seepage Meters and Mini-piezometers. *Journal of Geological Education* 27: 6–10.

Lunt I.A., Bridge J.S. & Tye R.S. 2004. Development of a 3-D depositional model of braided-river gravels and sands to improve aquifer characterization. *SEPM Special Publication* No. 80: 139–169.

Marimuthu S., Reynolds D.A. & La Salle C.L.G. 2005. A field study of hydraulic, geochemical and stable isotope relationships in a coastal wetlands system. *Journal of Hydrology* 315: 93–116.

Marttunen M., Hellsten S., Kerätär K., Tarvainen A., Visuri M., Ahola M., Huttunen M., Suomalainen M., Ulvi T. & Vehviläinen B. 2004. *Kemijärven säännöstelyn kehittäminen–yhteenveto ja suositukset*. Lapin ympäristökeskus, Suomen ympäristökeskus, pp 236, available at http://hdl.handle.net/10138/40472.

Meinzer O.E. 1923. *The occurrence of ground water in the United States, with a discussion of principles*. Water Supply Paper 489, Washington, DC, available at http://pubs.er.usgs.gov/publication/wsp489.

Merlivat L. & Jouzel J. 1979. Global climatic interpretation of the deuterium-oxygen 18 relationship for precipitation. Journal of Geophysical Research: *Oceans* 84: 5029–5033.

Moroizumi T., Ito N., Koskiaho J. & Tattari S. 2014. Long term trends of pan evaporation and an analysis of its causes in Finland. *SYKE-OU Project Report*: 23–46.

Nimmo J.R., Horowitz C. & Mitchell L. 2015. Discrete-storm water-table fluctuation method to estimate episodic recharge. *Ground Water* 53: 282–292.

Niswonger R.G., Panday S. & Ibaraki M. 2011. *MODFLOW-NWT, a Newton formulation for MODFLOW-2005*. US Geological Survey Techniques and Methods 6-A37, 44 pp.

Pääkkö E. 2004. Keski-Lapin aapasoiden luonto. *Metsähallituksen luonnonsuojelujulkaisuja. Sarja A* 145: 153 pp.

Poeter E., Hill M., Lu D., Tiedeman C. & Mehl S. 2014. *UCODE_2014, with new capabilities to define parameters unique to predictions, calculate weights using simulated values, estimate parameters with SVD, evaluate uncertainty with MCMC, and more*. International Ground Water Modeling Center Report Number GWMI 2014-02, available at http://igwmc.mines.edu/freeware/ucode/.

Price J. & Maloney D. 1994. Hydrology of a patterned bog-fen complex in southeastern Labrador, Canada. *Hydrology Research* 25: 313–330.

Price J., Maloney D. & Downey F. 1991. Peatlands of the Lake Melville coastal plain, Labrador. In: *Northern Hydrology: Selected Perspectives Proceedings of the Northern Hydrology Symposium*, pp. 293–302.

Pulkkinen E. 1983. *Sattasen karttalehtialueen geokemiallisen kartoituksen tulokset*. Geologinen tutkimuslaitos, Espoo, available at http://tupa.gtk.fi/kartta/geokemiallinen_karttaselitys/gks_3714_s.pdf.

Räisänen J. 2014. *Sodankylän alueen maaperäkartoitus 2013–2014 (Väliraportti)*. Archive Report 52/2014, Geological Survey of Finland, available at tupa.gtk.fi/raportti/arkisto/52_2014.pdf.

Rautio A. 2015. *Groundwater−surface water interactions in snow-type catchments: integrated resources*. PhD thesis, University of Helsinki, Helsinki.

Rautio A. & Korkka-Niemi K. 2015. Chemical and isotopic tracers indicating groundwater/surface-water interaction within a boreal lake catchment in Finland. *Hydrogeology Journal* 23: 687–705.

Rautio A., Korkka-Niemi K.I. & Salonen V.-P. 2018. Thermal infrared remote sensing in assessing groundwater and surface-water resources related to Hannukainen mining development site, northern Finland. *Hydrogeology Journal* 26: 163–183.

Rautio A., Kivimäki A.-L., Korkka-Niemi K., Nygård M., Salonen V.-P., Lahti K. & Vahtera H. 2015. Vulnerability of groundwater resources to interaction with river water in a boreal catchment. *Hydrology Earth System Sciences* 19: 3015-3032.

Reeve A., Siegel D. & Glaser P. 2000. Simulating vertical flow in large peatlands. *Journal of Hydrology* 227: 207–217.

Ruuhijärvi R. & Lindholm T. 2006. Ecological gradients as the basis of Finnish mire site type system. *The Finnish Environment* 23: 119–126.

Saarnisto M. 1992. The postglacial history of Kemijoki. *Special Paper — Geological Survey of Finland* 15: 151–159.

Sallantaus T. 2006. Mire ecohydrology in Finland. In: Lindholm T. & Heikkilä R. (eds.), *Finland: Land of Mires*, Finnish Environment Institute, Oulu, pp. 105–118.

Salonen V.-P., Korkka-Niemi K., Moreau J. & Rautio A. 2014. Kaivokset ja vesi — esimerkkinä Hannukaisen hanke. *Geologi* 66: 8–19.

Sauerbrey I.I. 1932. К вопросу о коэффициенте фильтрации грунтов и методике его исследования [In Russian]. On the Problem and Determination of the Permeability Coefficient [In English]. In: Proceedings VNIIG 3–5.

Sibson R. 1981. A Brief Description of Natural Neighbor Interpolation. In: Bannett V. (ed.), *Interpolating multivariate data*, John Wiley & Sons, New York, pp. 21-36.

Siegel D.I. 1988. The Recharge-Discharge Function of Wetlands Near Juneau, Alaska: Part I. Hydrogeological Investigations. *Groundwater* 26: 427–434.

Solantie R. 2006. Climate of Finland and its effect on mires. In: Lindholm T. & Heikkilä R. (eds.), *Finland – land of mires*, Finnish Environment Institute, Oulu, pp. 17–22.

Solantie R. & Ekholm M. 1985. Water balance in Finland during the period 1961–1975 as compared to 1931–1960. *Vesientutkimuslaitoksen julkaisuja* 59: 24–53.

Sophocleous M. 2002. Interactions between groundwater and surface water: the state of the science. *Hydrogeology Journal* 10: 52–67.

Stober I. & Bucher K. 2015. Hydraulic conductivity of fractured upper crust: insights from hydraulic tests in boreholes and fluid-rock interaction in crystalline basement rocks. *Geofluids* 15, No. 1-2: 161–178.

Stoneman D.A. & Constantz J. 2003. *Heat as a tool for studying the movement of ground water near streams*. US Department of the Interior, US Geological Survey.

Suonperä E. 2016. *Holocene paleohydrology of Viiankiaapa mire, Sodankylä, Finnish Lapland*. MSc Thesis, Univer-

sity of Helsinki, Helsinki.

Therrien R., McLaren R., Sudicky E. & Panday S. 2010. *HydroGeoSphere: A three-dimensional numerical model describing fully-integrated subsurface and surface flow and solute transport*. Groundwater Simulations Group, University of Waterloo, Waterloo, ON.

Torgersen C.E., Faux R.N., McIntosh B.A., Poage N.J. & Norton D.J. 2001. Airborne thermal remote sensing for water temperature assessment in rivers and streams. *Remote Sensing of Environment* 76: 386–398.

Triska F.J., Duff J.H. & Avanzino R.J. 1993. Patterns of hydrological exchange and nutrient transformation in the hyporheic zone of a gravel-bottom stream: examining terrestrial — aquatic linkages. *Freshwater Biology* 29: 259–274.

Tyrväinen A. 1980. *Suomen geologinen kartta 1:100 000: Lehti = Sheet 3714. Sattanen kallioperäkartta = Geological map of Finland 1:100 000; Pre-Quaternary rocks*. Geologinen tutkimuslaitos.

Tyrväinen A. 1983. *Suomen geologinen kartta 1:100 000: Lehdet = Sheets 3713 ja 3714. Sodankylän ja Sattasen kartta-alueiden kallioperä = Pre-Quaternary rocks of the Sodankylä and Sattanen map-sheet areas kallioperäkarttojen selitykset = Geological map of Finland 1:100 000; explanation to the maps of pre-Quaternary rocks*. Geologinen tutkimuslaitos, Espoo.

Ulvinen T. 2009. Hamatocaulis vernicosus – vaarantunut. In: Laaka-Lindberg S., Anttila S. & Syrjänen K. (eds.), *Suomen uhanalaiset sammalet*, Suomen ympäristökeskus, pp. 119–121.

Ulvinen T. & Sallantaus T. 2009. Hamatocaulis lapponicus – erittäin uhanalainen. In: Laaka-Lindberg S., Anttila S. & Syrjänen K. (eds.), *Suomen uhanalaiset sammalet*, Suomen ympäristökeskus, pp. 118–119.

Vehviläinen B. 2007. Hydrological Forecasting and Real-Time Monitoring: The Watershed Simulation and Forecasting System (WSFS). In: Heinonen P., Ziglio G. & Beken A.V.D. (eds.), *Hydrological and Limnological Aspects of Lake Monitoring*, Water Quality Measurements Series, John Wiley & Sons, Ltd., pp. 13–20.

Vukovic M. & Soro A. 1992. *Determination of Hydraulic Conductivity of Porous Media from Grain-Size Composition*. Water Resources Publication, Colorado, USA.

Weiss M. & Gvirtzman H. 2007. Estimating Ground Water Recharge using Flow Models of Perched Karstic Aquifers. *Groundwater* 45: 761–773.

Winter T.C. 1999. Relation of streams, lakes, and wetlands to groundwater flow systems. *Hydrogeology Journal* 7: 28–45.

Woessner W.W. 2000. Stream and Fluvial Plain Ground Water Interactions: Rescaling Hydrogeologic Thought. *Groundwater* 38: 423–429.

Younger P.L. & Wolkersdorfer C. 2004. Mining Impacts on the Fresh Water Environment: Technical and Managerial Guidelines for Catchment Scale Management. *Mine Water and the Environment* 23: 2–80.
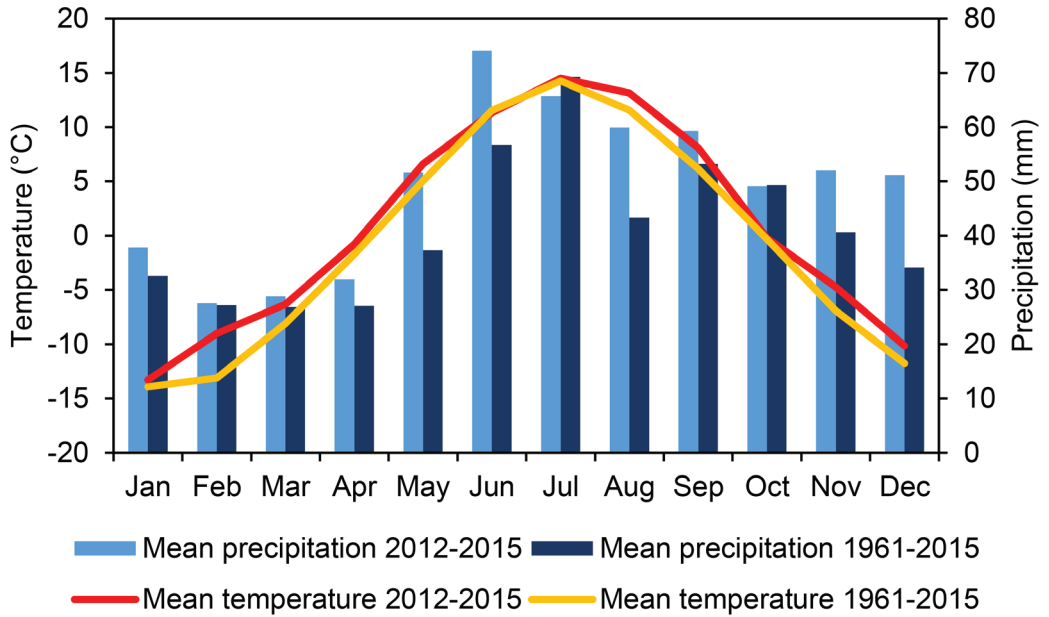
Appendix

Fig. A1. Monthly mean temperatures and precipitation in Sodankylä. Mean temperatures and precipitation were slightly higher during the 2012–2015 period than the 1961–2015 period.
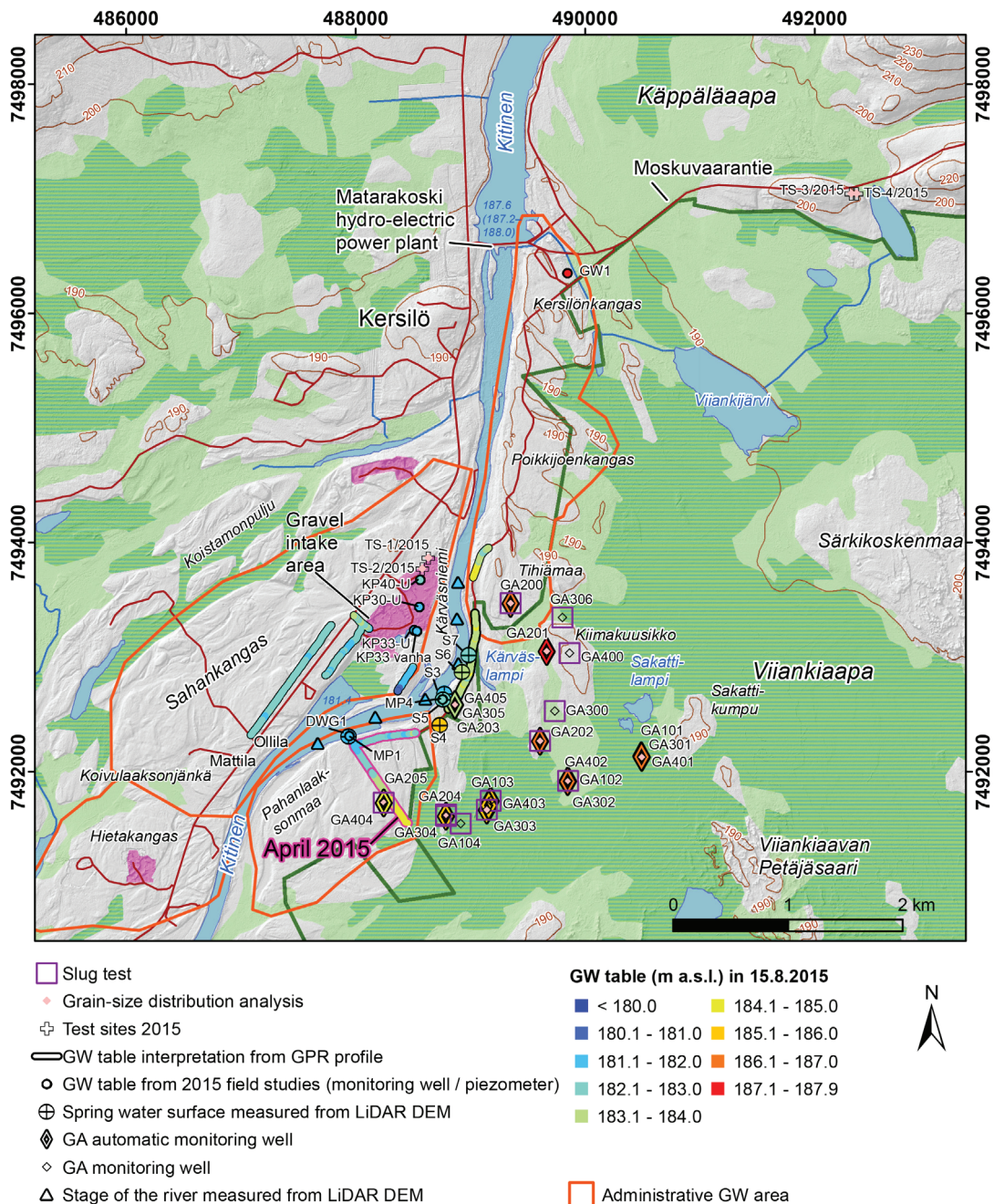
Fig. A2. Locations of sediment samples and slug tests used to calculate the hydraulic conductivities, GW tables in monitoring wells and GPR profiles performed in August and April 2015 and measurements from LiDAR DEM (the surface of River Kitinen). All measurements were carried out in August, except for the pink-outlined GPR interpretations. The well triplets of Golder Associates (GA) are also referred to as GA203, GA305 and GA405 (triplet 5), wells GA101, GA301 GA401 (triplet 1), wells GA101, GA302 and GA402 (triplet 2) and the GA103, GA303 and GA403 (triplet 3). Terrain elements were reproduced with permission from the copyright owner (National Land Survey of Finland). Administrative GW area was reproduced with permission from the copyright owner (Finnish Environment Institute).
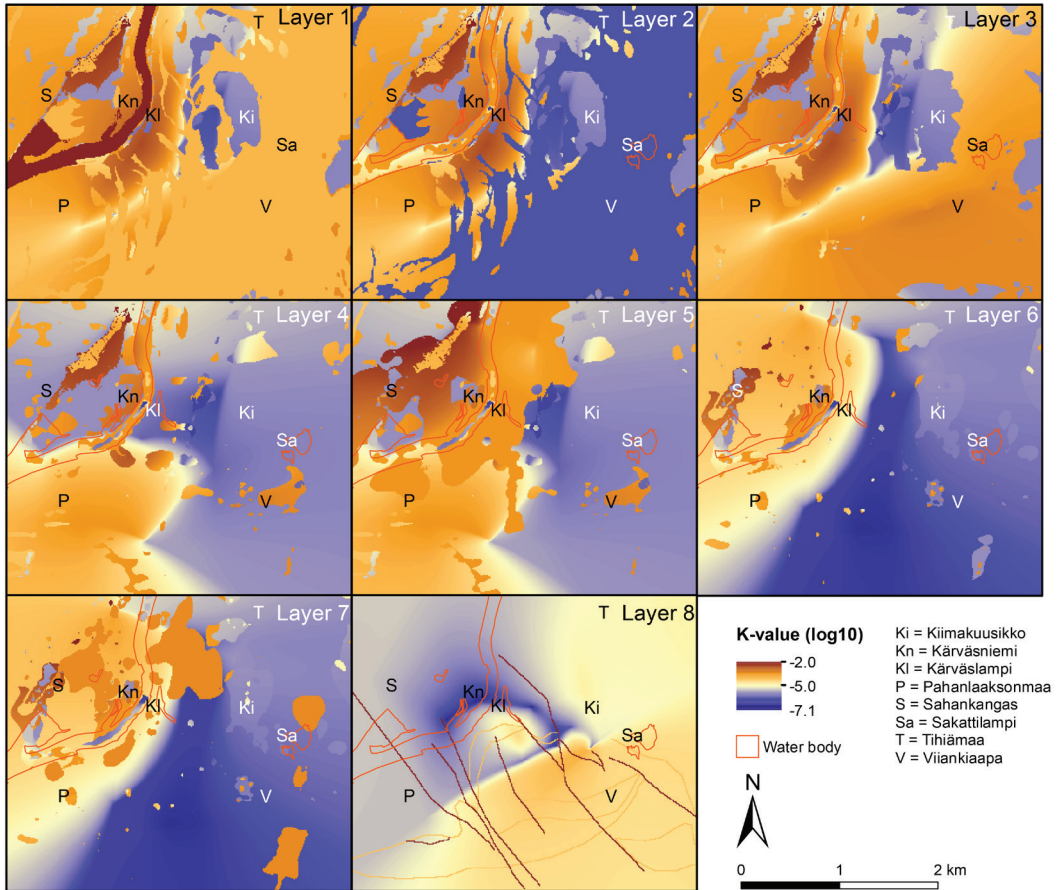
Fig. A3. The horizontal *k*-values of the hydrostratigraphic units of the GW flow model defined based on the expected geology. The *k*-values are presented on a log-10 scale. Water bodies were reproduced with permission from the copyright owner (National Land Survey of Finland).

Table A1. The $\delta^{18}O$, δD and *d*-excess values of water samples in 2015 and 2016.

ID	Date	$\delta^{18}O$, VSMOW (‰)	δD, VSMOW (‰)	*d*-excess (‰)
KP40–U	7 Aug. 2015	−13.29	−99.2	7.1
KP31	7 Aug. 2015	−12.00	−89.8	6.2
KP30–U	7 Aug. 2015	−13.62	−103.1	5.9
GA305	8 Aug. 2015	−13.74	−103.1	6.8
GA203	8 Aug. 2015	−13.80	−103.7	6.7
GA405	8 Aug. 2015	−12.50	−96.2	3.8
GA200	8 Aug. 2015	−12.74	−98.1	3.9
GA300	9 Aug. 2015	−14.01	−103.0	9.1
GA202	9 Aug. 2015	−14.30	−107.0	7.4
GA202 deep	9 Aug. 2015	−14.30	−107.1	7.3
GA201	9 Aug. 2015	−13.98	−103.4	8.5
GA400	9 Aug. 2015	−14.61	−108.1	8.8
GA100	9 Aug. 2015	−10.26	−83.7	−1.6
GA306	9 Aug. 2015	−14.23	−105.7	8.2
GA404	10 Aug. 2015	−14.25	−105.2	8.8
GA103	14 Sep. 2016	−12.50	−95.8	4.2
GA403	14 Sep. 2016	−12.08	−94.0	2.6
GA303	14 Sep. 2016	−12.32	−94.0	4.6
GA102	14 Sep. 2016	−11.29	−86.3	4.0
GA302	14 Sep. 2016	−12.72	−97.9	3.9
GA402	14 Sep. 2016	−12.75	−98.1	3.9
SPRING3	10 Aug. 2015	−13.64	−102.9	6.3
SPRING4	10 Aug. 2015	−10.53	−83.6	0.7
SPRING5	11 Aug. 2015	−12.78	−97.6	4.6
SPRING6	11 Aug. 2015	−10.40	−84.3	−1.1
SPRING7	11 Aug. 2015	−9.88	−78.4	0.6
SW1	7 Aug. 2015	−12.25	−95.9	2.1
SW3	8 Aug. 2015	−12.01	−90.2	5.9
SW4	10 Aug. 2015	−9.16	−73.5	−0.2
SW7	11 Aug. 2015	−9.62	−75.3	1.6
SW8	11 Aug. 2015	−12.24	−91.9	6.0
SW9	11 Aug. 2015	−9.63	−75.3	1.7
MP1	8 Aug. 2015	−14.20	−106.9	6.7
MP3	15 Aug. 2015	−13.00	−99.4	4.6
MP4	15 Aug. 2015	−11.94	−92.5	3.1
DGW1	10 Aug. 2015	−12.28	−92.3	5.9